Material Matters™

Vol. 4, No. 2

ALDRICH Chemistry

Advanced Ceramics

Materials and Applications

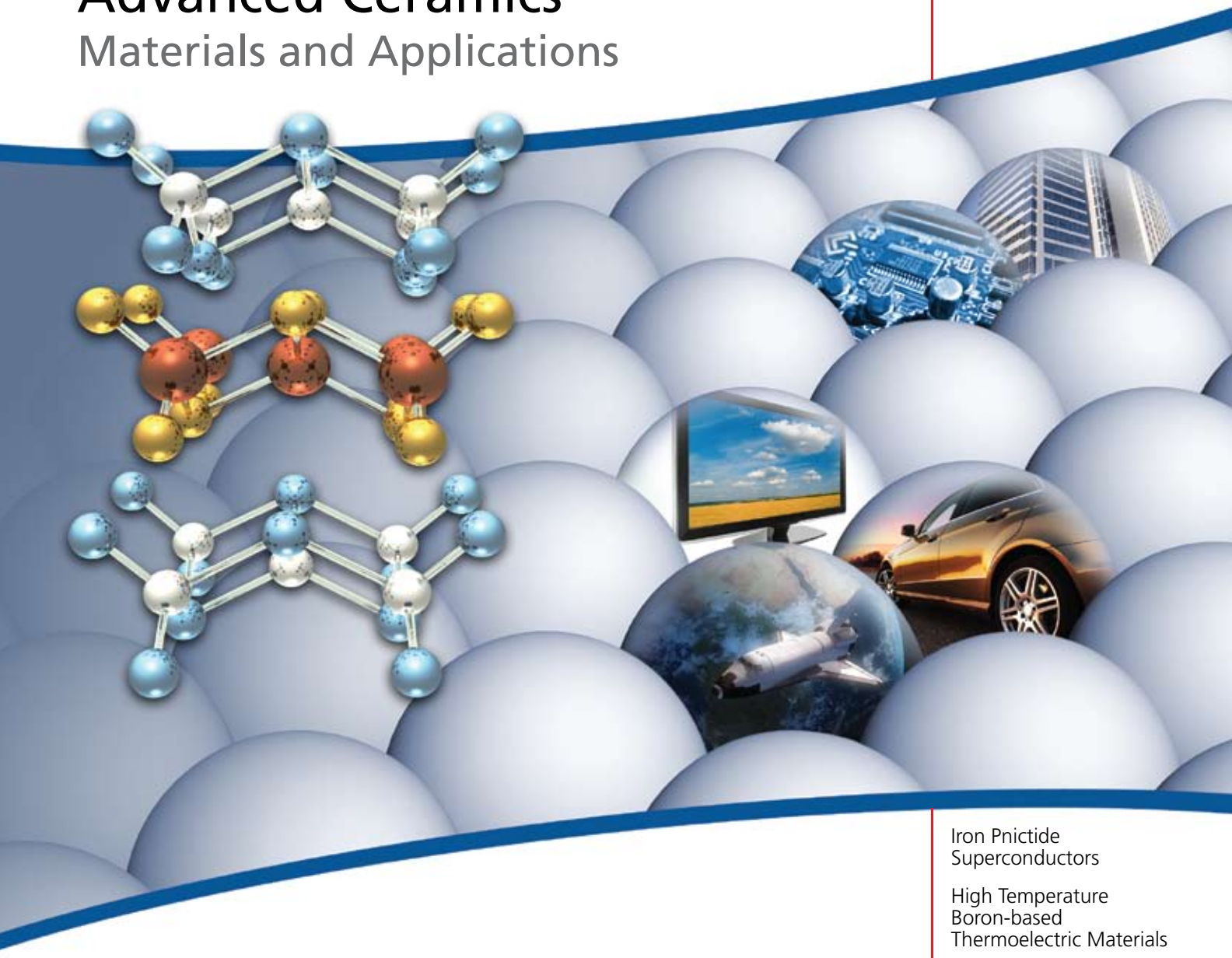

Ceramics—more than just common materials

Iron Pnictide Superconductors

High Temperature Boron-based Thermoelectric Materials

Silicon Carbide

Mesoporous Oxides and Their Applications to Hydrogen Storage

Introduction

Viktor Balema, Ph.D.
Materials Science
Sigma-Aldrich Corporation

Ceramics can be broadly defined as nonmetallic inorganic solids consisting of infinite arrays of metal and nonmetal ions. The arrays do not form discrete units such as molecules or polymeric chains. As a rule, ceramics combine metal oxides, borides, carbides, arsenides, nitrides or other inorganic compounds into complex materials which have properties that differ considerably from those of the original constituents.

The name "ceramic" originates from the Greek word "keramos", which means "pottery". It can also be traced back to the word "Shrapika" meaning "potter" in Sanskrit.[1] For centuries, ceramic materials were manufactured by firing clay precursors, and most of the common ceramic products, such as tiles, cookware and bricks are still made this way.

Constantly growing demand for advanced materials in the 20th century resulted in the development of new classes of ceramic materials that do not originate in clays. Such materials, known as "Advanced Ceramics", are manufactured either from pure metal oxides by ceramic forming techniques,[2] or from other precursors using sol-gel processing,[3] atomic layer deposition,[4] or gas-phase synthesis.[5] It wouldn't be an exaggeration to say that advanced ceramics play a crucial role in most areas of modern science and technology. Their applications comprise electronic materials and devices, nanomaterials, coatings, structural materials and composites.

Alternative energy is an area where advanced ceramics have proven to be particularly valuable. For example, high-temperature superconducting ceramic materials demonstrate great potential for reducing energy losses in electrical systems and devices, thus increasing their energy efficiency. Thermoelectric ceramics are capable of clean energy generation by transforming waste heat into electricity. Highly porous complex oxide systems find use as media for safe storage of energy rich gases such as hydrogen. Ceramics are also used as substrates for light emitting diodes, electrodes and electrolytes for solid oxide fuel cells (SOFC), highly efficient insulators etc.

The current issue of *Material Matters* features four articles that are concerned with applications of advanced ceramic materials in alternative energy and electronics fields. The issue begins with an article by Hideo Hosono from Tokyo Institute of Technology, Tokyo, Japan, that highlights novel superconducting ceramic materials recently developed by his group. Novel thermoelectric ceramics are discussed in the paper by Takao Mori from National Institute for Materials Science, Tsukuba, Japan, and silicon carbide based materials are reviewed in the article by Nicholas Wright and Alton B. Horsfall from Newcastle University, Newcastle, UK. Finally, the group led by Samuel Mao from the Lawrence Berkeley National Laboratory, USA, reports on the properties of nanoporous oxides for hydrogen storage and other energy related applications. The issue also highlights Aldrich Materials Science products for solid oxide fuel cell (SOFC) applications as well as ceramic nanomaterials, high-purity metal oxides and precursors for vapor deposition of ceramic thin films.

Customary to *Material Matters*, each article in this issue is accompanied by Sigma-Aldrich® products helpful in the corresponding type of advanced ceramics research. The facing page lists the materials categories that you will find in this issue. Please visit Aldrich Materials Science at *sigma-aldrich.com/matsci* for product information. We invite you to send your comments and questions regarding *Material Matters* and materials of interest to *matsci@sial.com*.

References:

(1) http://www.iitk.ac.in/infocell/Archive/dirjuly3/techno_ceramics.html (last accessed May 5, 2009)
(2) Carter, C.B., Norton, M.G. *Ceramic Materials*, Springer: New York, London, 2007.
(3) *Material Matters* **2006**, *1*, 3, 8-9.
(4) *Material Matters* **2008**, *3*, 2, 28-30.
(5) *Material Matters* **2009**, *4*, 1, 2-4.

About Our Cover

Ceramic materials have always been, and will continue to be, an inseparable part of human life. They are essential constituents in all modern technologies and devices including computers, displays, cars and spacecraft among others. Due to their unique combination of properties such as hardness, durability, high electrical and thermal resistivity and magnetic behavior, ceramic materials have become irreplaceable in a broad variety of applications. The most striking among them is the ability of certain complex ceramics to completely lose their electrical resistance at relatively high temperatures—an effect known as high-temperature superconductivity. The structure on the cover represents a group of high-temperature superconductors with the general formula LaFeAsO, developed at the Tokyo Institute of Technology. Read about these unique materials in Dr. Hosono's article on the pages 32-35.

Material Matters™
Vol. 4 No. 2

Aldrich Chemical Co., Inc.
Sigma-Aldrich Corporation
6000 N. Teutonia Ave.
Milwaukee, WI 53209, USA

To Place Orders

Telephone	800-325-3010 (USA)
FAX	800-325-5052 (USA)

Customer & Technical Services

Customer Inquiries	800-325-3010
Technical Service	800-231-8327
SAFC®	800-244-1173
Custom Synthesis	800-244-1173
Flavors & Fragrances	800-227-4563
International	414-438-3850
24-Hour Emergency	414-438-3850
Web site	sigma-aldrich.com
Email	aldrich@sial.com

Subscriptions

To request your **FREE** subscription to *Material Matters*, please contact us by:

Phone: **800-325-3010** (USA)

Mail: **Attn: Marketing Communications**
Aldrich Chemical Co., Inc.
Sigma-Aldrich Corporation
P.O. Box 355
Milwaukee, WI 53201-9358

Website: **sigma-aldrich.com/mm**
Email: **sams-usa@sial.com**

International customers, please contact your local Sigma-Aldrich office. For worldwide contact information, please see back cover.

Material Matters is also available in PDF format on the Internet at ***sigma-aldrich.com/matsci***.

Material Matters (ISSN 1933–9631) is a publication of Aldrich Chemical Co., Inc. Aldrich is a member of the Sigma-Aldrich Group.

"Your Materials Matter."

Joe Porwoll, President
Aldrich Chemical Co., Inc.

Do you have a compound that you wish Sigma-Aldrich® could list to help materials research? If it is needed to accelerate your research, it matters—please send your suggestion to ***matsci@sial.com*** *and we will be happy to give it careful consideration.*

Prof. Padma Gopalan of the University of Wisconsin, Madison, kindly suggested that we offer ferrocenylmethyl methacrylate (**Aldrich Prod. No. 700479**). The incorporation of metal containing moieties in block copolymer architecture lays the foundation for the inclusion of new functionalities to nanostructured materials. Examples include the incorporation of redox-active, photophysical, conductive, catalytic, or pre-ceramic functionalities. Polymers containing Ferrocene (**Aldrich Prod. No. F408**) have been widely used, largely due to their redox-induced morphological changes, their ability to serve as precursors for magnetic or catalytic materials and their use as plasma etch-resistant nano-templates. Ferrocenylmethyl methacrylate can be polymerized by a number of controlled radical polymerization techniques, which provide simple synthetic routes to a variety of functional polymers.

Ferrocenylmethyl methacrylate, 95% (NMR)

FMMA
[31566-61-7] $C_{15}H_{16}FeO_2$ FW 284.13

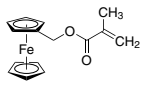

mp 52 to 54 °C

700479-1G	1 g

References:

(1) Rider, D. A.; Liu, K.; Eloi, J.-C.; Vanderark, L.; Yang, Ling.; Wang, J.-Y.; Grozea, D.; Lu, H.-Z.; Russel, T.P.; Manners, I. *ACS Nano* **2008**, *2(2)*, 263.
(2) Sakakiyama, T.; Ohkita, H.; Ohoka, M.; Ito, S.; Tsujii, Y.; Fukuda. T. *Chem. Lett.* **2005**, *34*, 1366.

Advanced Ceramics and Other Materials Featured in this Issue*

*Products within each table are sorted by the atomic number of the first element where applicable.

Iron Pnictide Superconductors: Discovery and Current Status

Hideo Hosono[1,2]*

1. Frontier Research Center & Materials and Structures Laboratory
Tokyo Institute of Technology
Nagatsuta 4259, Midor-ku, Yokohma
226-8503
2. Transparent Functional Oxide Project, ERATO-SORST
Japan Science and Technology Agency
Japan
*Email: hosono@msl.titech.ac.jp

Introduction

In general, oxides of representative metals are the most abundant and stable materials on earth, and they are also environmentally friendly. Although they are not believed to become electron-active materials, and although they have been used as ingredients in traditional materials such as cement, glass, and porcelain, only a few active functions have been found for them. In fact, college textbooks describe the materials listed above as typical insulators. However, a widely accepted view that "a transparent oxide cannot be a platform for electro-active materials" comes only from phenomenological observation. We think it possible to realize a variety of active functionalities in transparent oxides through appropriate approaches based on deep insight into the electronic structures of these oxides. Therefore, we have concentrated on material exploration and device application of transparent oxide semiconductors (TOSs).[1]

We have explored novel transparent oxide semiconductors, focusing on the low dimensional structure embedded in the crystal structure: in particular, a 3-dimensionally (3D) connected nanometer sized cage structure and a 2-dimensional (2D) layered structure composed of a narrow gap semiconductor material layer sandwiched between wide-gap insulating layers. We expect an emergence of unique electronic properties resulting from a low-dimensional electronic state.

A typical example obtained from the 3D-connected sub-nanometer-sized cage structure is the conversion of refractory oxide $12CaO{\cdot}7Al_2O_3$ (C12A7) into both a transparent semiconductor and a metallic conductor by electron-doping through a conduction band composed of 3D-connected sub-nanometer-sized cages. This material is a band insulator with a band gap of ~7eV, and it is a known constituent of alumina cement. Three-dimensionally connected sub-nanometer-sized cages with a positive charge form another conduction band which is located ~2eV below the conduction band primarily composed of 5s-orbitals of Ca ions constituting cage walls. While electron-doping to the cage wall conduction band is impossible due to low electron affinity, the cage conduction band allows it to be doped by other methods. When the doped electron concentration reaches ~$1x10^{21}$ cm^{-3}, an insulator-metal transition is observed, and the metallic C12A7 exhibits a superconducting transition at 0.2-0.4K. This means a cement superconductor has been realized![2]

A representative example obtained from the latter structure is a transparent P-type semiconductor LaCuOCh (where Ch=S and Se). Lack of P-type material posed a major obstacle in TOSs for extension as transparent oxide electronics. In 1997, we reported the first p-type TOS, $CuAlO_2$, with a layered structure and a chemical design concept.[3] Although the discovery of a series of p-type TOSs led to the realization of current-injection, ultraviolet-emission from Pn heterojunctions composed of all TOSs (e.g., p-$SrCu_2O_2$/n-ZnO) in 2000, performance of p-type TOS must be improved for more realistic applications. We chose LaCuOCh as the candidate material. This material belongs to the tetragonal lattice category and is composed of alternatively stacked semi-conductive $(CuCh)^-$ and insulating $(LaO)^+$ layers. Since the location of the valence band maximum and the conduction band minimum is different between bulk $CuCh_2$ and La_2O_3, we expect to statically separate the carrier transport layers from the impurity-doped layer.

Electromagnetic Properties of LaT_MPnO

When a pnicogen anion (Pn) with -3 charge replaces a chalcogen anion (Ch) with -2 charge in LaCuOCh, a transition metal cation (T_M) with +2 can substitute for Cu^+ with $3d^{10}$ electronic configuration. Many intermetallic compounds exist between T_M and Pn, and they have various magnetic properties. Thus, we expected to find intriguing electromagnetic properties arising from the 2-dimensional electronic structure of T_MPn in the compound LaT_MPnO. This was the motivating force to research this series of compounds.

Figure 1 summarizes the electromagnetic properties of LaT_MPnO that have been clarified to date.[3] The electromagnetic properties drastically vary with the number of 3d electrons in T_M; Mn is anti-ferromagnetic (AF) semiconductors while Co is a ferromagnetic (FM) metal, and Ni is a paramagnetic metal at ambient temperature and superconconductor at low temperatures.[4] At the same time, when T_M is Fe, the properties of P and As based systems are also different. LaFePO is a paramagnetic metal exhibiting a superconducting transition at 4K. This behavior is almost the same as that of LaNiOCh.

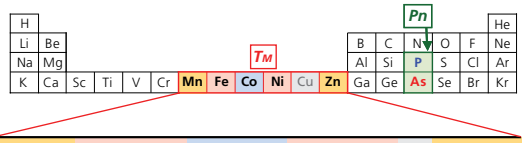

T_M^{2+}	$Mn(3d^5)$		$Fe(3d^6)$		$Co(3d^7)$		$Ni(3d^8)$		(Cu)	$Zn(3d^{10})$	
Pn	P	As	P	As	P	As	P	As		P	As
Elect. Prop.	Semiconductor		Superconductor		Metal		Superconductor		—	Semiconductor	
Magnetism	AFM				FM				—	Nonmagnetic	
E_g	~1 eV		—		—		—		—	~1.5 eV	
T_C / T_N	> 400 K		Undoped: 5 K	Undoped: X F-doped: 26 K	43 K	66 K	Undoped: 3 K	Undoped: 2.4 K		—	
Ref.	Yanagi et al. JAP submitted		Kamihara *et al.* JACS(2006), Kamihara *et al.* JACS (2008)		Yanagi et al. PRB (2008)		Watanabe *et al.* IC (2007), Watanabe *et al.* JSSC (in press)		—	Kayanuma *et al.* PRB (2007), Kayanuma *et al.* TSF (2008)	

Figure 1. Summary of electromagnetic properties in a LaT_MPnO system.

On the other hand, LaFeAsO exhibits a unique temperature dependence. It is a paramagnetic metal at high temperatures, but as the temperature decreases, a sudden decrease in resistivity and magnetic susceptibility occurs at ~160K, reaches a minimum, and then increases again as shown in **Figure 2**. No superconductive transition is observed. It is worth nothing that the system of T_M with an odd number of 3d electrons has a long-range spin ordering and does not exhibit superconductivity, whereas the system of T_M with an even number of 3d electrons is a paramagnetic metal exhibiting superconductivity. At this stage, we observed superconductivity only for LaFePO, Ca- or F-doped LaFePO,[5] and LaNiPnO (Pn=P and As).[6]

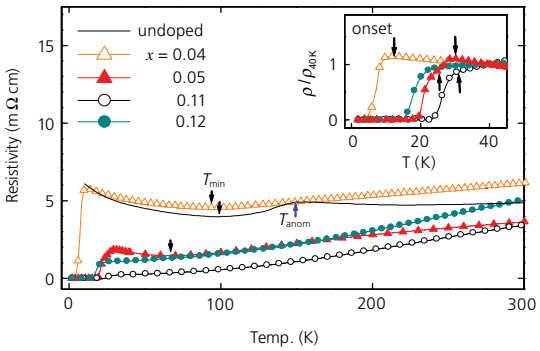

Figure 2. Temperature dependence of resistivity for $LaFeAsO_{1-x}F_x$ with x.

Emergence of T_C in LaFeAsO

Yoichi Kamihara, a postdoctoral fellow in charge of the Fe-system, attempted an aliovalent substitution of a doped carrier to LaFeAsO, following our previous experience with superconducting temperature (T_C) enhancement in LaFePO.[5] The result was marvelous! Although no noticeable change was seen upon the doping of Ca to the La sites, F-doping to the O-site induced a drastic change in the ρ-T curves as shown in **Figure 3.** As the F-content increases, the knick around 150K disappears, and zero-resistivity begins to appear at T> 4K for F>4 mol%. This temperature further increases up to 32K (onset) when fluorine content rises up to 11%. The observed zero-resistivity was confirmed as being due to superconductive transition in the bulk by measurements of magnetic susceptibility and heat capacity.

We noted that the emergence of T_c accompanies the disappearance of a sudden ρ-drop around 160K. Although T_C was found for LaFePO, LaNiPO, and LaNiAsO, we observed no such ρ-drop in any of them.

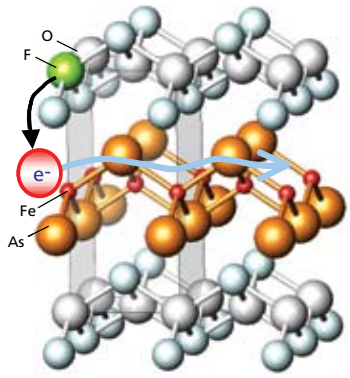

Figure 3. Crystal structure and role of F-doping in $LaFeAsO_{1-x}F_x$

What happens around 150K in LaFeAsO?

We assumed that the ρ-drop at ~150K was closely related to the emergence of high T_C. This could be due to spin-ordering or a crystallographic phase transition. Although neutron diffraction is the best technique to check this possibility, we needed a lot of time to prepare the sample amount (~15g) to acquire reliable data. Thus, we measured X-ray diffraction as soon as we could and obtained a beam time for the low-temperature powder XRD at Spring-8 as courtesy of Dr. Masaki Takata of RIKEN. The results of the XRD shown in **Figure 4** were unambiguous.[4] Crystallographic transition from tetragonal (Space group: *P4/nmm*) to orthorhombic phase (*Cmma*) was observed at ~155K for the un-doped sample, but no such transition was observed for the F-doped, superconductive samples. A two-peak structure was observed in the heat-capacity measurement of the un-doped sample. The location of the high temperature peak agrees with that of the crystallographic transition.

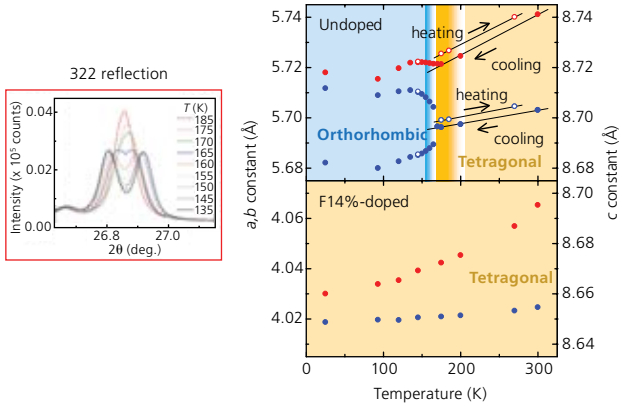

Figure 4. (Left) change in X-ray diffraction 322 peak of undoped LaFeAsO with temperature. (Right) Lattice constants of undoped and F14%-doped LaFeAsO as a function of temperature.

Local probe techniques, NMR on ^{139}La, and a Mossbauer spectroscopy of ^{57}Fe provided different information. Both measurements revealed that anti-ferromagnetic ordering occurred at ~145K, corresponding with the low-temperature heat capacity peak. But when electron carriers were doped, anti-ferromagnetic ordering continuously decreases and T_C appears, reaches a max, and then decreases. **Figure 5** is an electronic phase diagram of this system.

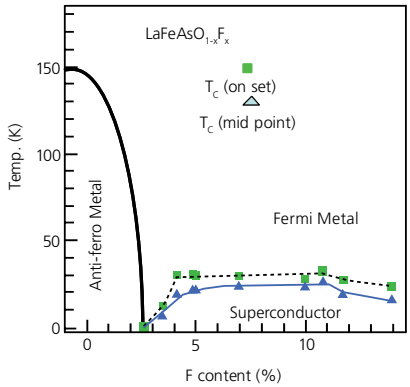

Figure 5. Electronic phase diagram of $LaFeAsO_{1-x}F_X$

A Brief History of Fe(Ni)-Based Superconductors

Since our report on $LaFeAsO_{0.9}F_{0.1}$ with T_C=26K, more than 500 papers have been published in peer-reviewed journals, and more than 300 unpublished manuscripts have been posted on preprint servers. **Figure 6** summarizes the milestone papers focused on materials as a function of the received date (or posted date for the preprint).[4] The Takahashi Group of Nihon University and our group submitted a paper [8] at the end of February 2008 that applying high pressure results in a steep increase in the T_C of $LaFeAsO_{0.9}F_{0.1}$ to 43K at 4GPa.This T_C was the highest, with the exception of cuprates, among all superconductors reported so far. The high sensitivity of superconducting temperature to pressure quickly manifested as the replacement of the La ion with the largest ionic radius among the rare-earth ions because the replacement of a larger-sized ion with a smaller-sized ion leads to the chemical pressure effect on the structure. Several Chinese groups (Chinese Academy of Science, U. Sci.&Tech. China) performed a series of excellent works; X.H. Chen et. al. (USTC) reported T_C=43K on March 25 for $SmFeAsO_{1-x}F_X$. On March 26, G.F. Chen et. al. (CAS) posted T_C =41K for $CeFeAsO_{1-x}F_X$. Ren et. al. (CAS) posted T_C=52K for $PrFeAsO_{1-x}F_X$ on March 29, and posted T_C=55K for $SmFeAsO_{1-x}F_x$ on April 13. Ren et al.[9] in CAS first proposed the effectiveness of high-pressure synthesis. Electron-doping was possible via the formation of oxygen vacancy instead of substituting F for O-sites. Synthesis at higher temperatures resulted in the improvement of crystalline quality of ReFeAsO, but the maximum temperature attainable was limited to ~1150 °C by the softening of a silica glass tube used as a conventional reaction vessel. High-pressure synthesis removed this limitation because it uses a BN vessel instead of a silica glass tube.

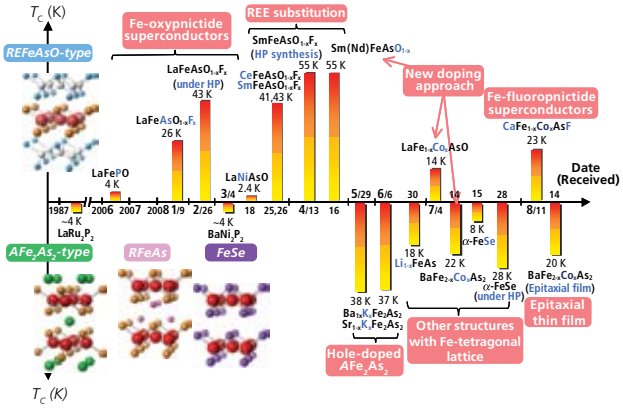

Figure 6. Progress in Fe(Ni)-based superconductors

Sefat et. al.[10] a Tennessee group, recently reported an interesting doping method: electron-doping by substitution of the Fe^{2+} ($3d^6$) sites with Co^{2+} ions ($3d^7$). This doping method was surprising because replacement of Cu^{2+} with other transition metal cations in cuprates largely reduces T_C. A T_C robust enough to substitute for Fe ion sites is quite unique for Fe pnictide superconductors, and lends greater flexibility to a carrier doping method for inducing superconductivity.

It is a natural idea to explore the superconductivity in multi-layered T_MPn for high T_C if you know the history of high T_C cuprates. The first report on superconductivity in this type of material was on $LaRu_2P_2$ in 1987 by Jeitschko et al.[11] Mine et al.[12] who reported a T_C of 4K in $BaNi_2P_2$ with a bi-layered structure on March 3. Temperature dependence of resistivity has no anomaly around 150K like that of LaNiPnO or LaFePO. On July 17, Rotter et al.[13] reported T_C of 38K in $Ba_{1-x}K_xFe_2As_2$. The parent material $BaFe_2As_2$ has properties similar to LaFeAsO with respect to crystallographic transition from the tetragonal (*I4/mmm*) to orthorhombic (*Fmmm*) phase at 140K, ρ-T curve, and AF transition. It is phenomenologically obvious from the comparison between $BaNi_2P_2$ and $BaFe_2As_2$ that to achieve the high T_C the parent phase experiences a crystallographic transition at higher temperatures accompanying AF-ordering. Charge carrier types effective for the emergence of superconductivity in this series of materials appeared to be the reverse of the Fe oxypnictides: hole doping works well for the former, whereas electron-doping does for the latter. Although the effective charge carrier for inducing superconductivity is different, the phase diagram in the Fe-pnictides is close to that in the cuprates.

The common structural unit in ReFeAsO and $BaFe_2As_2$ is the square lattice of Fe. Hsu et al.[14] reported superconductivity at 8K in β-FeSe with a PbO-type structure on July 15. This material with tetragonal symmetry at RT has the simple crystal structure consisting of infinite stacking FeSe layers in which Fe forms a square lattice. An increase in T_C of β-FeAs after applying high pressure to a maximum of 28K was posted on July 28.

Perspective: Strike While the Iron is Hot

Table 1 summarizes the properties of three representative families of superconductors. A number of similarities have been reported between Fe-based superconductors and cuprates. However, there are two distinct differences between the two groups of materials: the nature of the parent phase and the robustness to element substitution. The parent phase of high T_C-cuprates is a Mott insulator, characterized by high repulsive energy among Cu 3d electrons, U_{dd}, whereas the mother phase of the Fe-based superconductors appears to be metal. The highly delocalized nature of Fe 3d-electrons in the latter is consistent with the robustness of T_C upon replacing Fe with Co ions. We know that the band structure of the parent compound in the cuprates is largely altered by carrier (hole) doping. Description by a simple band model, i.e., the band structure of the parent material remains essentially unchanged even after carrier doping, is inappropriate due to strong electron correlation effects. On the other hand, the situation looks different for the Fe system. According to a recent evaluation by Malaeb et al,[15] the magnitude of U_{dd} for LaFeAsO is rather smaller than that of cuprates. If description by the rigid band models is effective for this system, increases in carrier electrons originating from Co^{2+} substituting at the Fe^{2+} site should lead to a similar result as F-substitution to the O-sites in LaFeAsO. The latter feature adds the possibility of discovering further candidate materials for new superconductors.

Table 1. Comparison of metal-based, high T_C superconductors

	Fe-oxypnictides	MgB_2	Cuprates
Parent Material	(bad) metal (T_N~150K)	metal	Mott Insulator (T_N~400K)
Fermi Level	3d 5-bands	2-bands	3d single band
Max T_C	56K	40K	~140K
Impurity effect	robust	sensitive	sensitive
S_C gap symmetry	extended-s-wave(?)	s-wave	d-wave
$Hc^2(0)$	100-200T>	~40T	~100T
J_C	?		

Figure 7 shows the T_C of some known superconductors versus the date of their discovery. The T_C in iron pnictide superconductors is second to high temperature cuprates, exceeding MgB_2, which has the maximum T_C of conventional metal superconductors which can be explained by the BCS theory (electron-pairing required for superconductivity is mediated by lattice vibrations).

We have experienced that the old saying is mostly correct: *"Strike while the iron is hot."* I hope cooperation and competition among active researchers will enhance the T_C of new superconductors toward the ultimate goal of room-temperature superconductors.

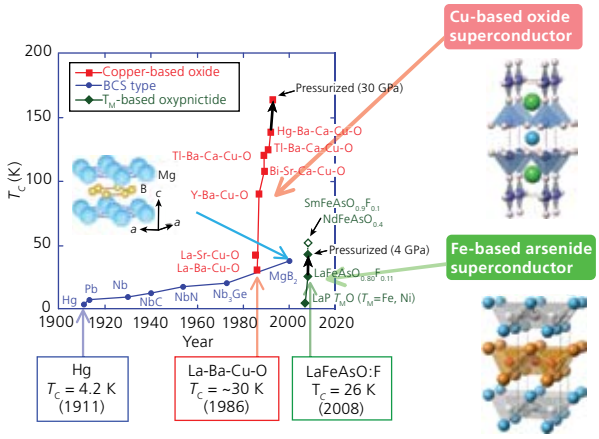

Figure 7. T_C of some known superconductors vs. the date of their discovery.

References:

(1) Hosono, H.; Kamiya, T.; Hirano, M. *Bull. Chem. Soc. Jpn*. **2006**, *79*.
(2) Miyakawa, M.; Kim, S.W.; Hirano, M.; Kohama, Y.; Kawaji, H.; Atake, T.; Ikegami, H.; Kono, K.; Hosono, H. *J. Am. Chem. Soc*., **2007**, *129,* 7270.
(3) Kawazoe, H.; Yasukawa, M.; Hyodo, H.; Kurita, M.; Yanagi, H.; Hosono, H. *Nature*, **1997**, *389*, 939.
(4) Hosono, H. *J. Phys. Soc. Jpn*., **2008**, *77SC*, 1.
(5) Kamihara, Y.; Hiramatsu, H.; Hirano, M.; Kawamura, R.; Yanagi, H.; Kamiya, T.; Hosono, H. *J. Am. Chem. Soc*., **2006**, *128,* 10012.
(6) Watanabe, T.; Yanagi, H.; Kamiya, T.; Kamihara, Y.; Hiramatsu, H.; Hirano, M.; Hosono, H. *Inorg. Chem*., **2007**, *46,* 7719.
(7) Kamihara, Y.; Watanabe, T.; Hirano, M.; Hosono, H.; *J. Am. Chem. Soc.,* **2008**, *130*, 3296.
(8) Takahashi, H.; Igawa, K.; Arii, K.; Kamihara, Y.; Hirano, M.; Hosono, H. *Nature,* **2008**, *453*, 376.
(9) Ren, Z.A.; Lu, W.; Yang, J.; Yi, W.; Shen, X.L.; Li, Z.C.; Che, G.C.; Dong, X.L.; Sun, L.L.; Zhou, F.; Zhao, Z.X. *Chin. Phys. Lett.*, **2008**, *25*, 2215.
(10) Sefat, A.S.; Mi, R.J.; McGuire, A.; Sales, B.C.; Singh, D.J.; Mandrus, D. *Phys. Rev. Lett.,* **2008**, *101*, 117004.
(11) Jeitschko, W.; Glaum, R.; Boonk, L. *J. Solid State Chem*., **1987**, *69*, 93.
(12) Mine, T.; Yanagi, H.; Kamiya, T.; Kamihara, Y.; Hirano, M.; Hosono, H. *Solid State Commun.*, **2008**, *147*, 111.
(13) Rotter, M.; Tegel, M.; Johrendt, D. *Phys. Rev. Lett*., **2008**, *101*, 107006.
(14) Hsu, F-C.; Luo, J-Y.; Yeh, K-W.; Chen, Ta-K.; Huang, T-W.; Wu, P-M. ; Lee, Y-C. ; Huang, Y-L. ; Chu, Y-Y. ; Yan, D-C. ; Wu, M-Ku. ; *Proc. Natl. Acad. Sci. U.S.A,*. **2008,** *105,* 14262.
(15) Malaeb, W.; Yoshida, T.; Kataoka, T.; Fujimori, A.; Kubota, M.; Ono, K.; Usui, H.; Kuroki, K.; Arita, R.; Aoki, H.; Kamihara, Y.; Hirano, M.; Hosono, H. *J. Phys. Soc. Jpn.,* **2008**, *77,* 093714.

Arsenides

For a complete list of metals, oxides, ceramics and related materials, please visit ***sigma-aldrich.com/ceramics***

Name	Formula	Purity	Dimensions	Physical Form	Cat. No.
Iron(III) arsenide	FeAs	99.5% trace metals basis	-	pieces	709018-1G
Zinc arsenide	Zn_3As_2	99.999% trace metals basis	-	pieces	709247-1G
Gallium arsenide	GaAs	99.999% trace metals basis	-	pieces	329010-1G 329010-5G
Gallium arsenide	GaAs	-	diam. × thickness 2 in. × 0.5 mm	<100> single crystal substrate	651486-1EA

Phosphides

Name	Formula	Purity	Dimensions	Physical Form	Cat. No.
Calcium phosphide	Ca_3P_2	-	1 - 7 mm	chunks	400971-100G 400971-500G
Iron phosphide	Fe_2P	99.5% trace metals basis	–40 mesh	powder	691658-5G
Iron phosphide	Fe_3P	99.5% trace metals basis	–40 mesh	powder	691593-5G
Nickel phosphide	Ni_2P	98%	–100 mesh	powder	372641-10G
Gallium phosphide	GaP	99.99% trace metals basis	-	chunks	521574-2G
Indium(III) phosphide	InP	99.998% trace metals basis	3 - 20 mesh	pieces	366870-1G

Ferrites

Name	Formula	Purity	Dimensions	Physical Form	Cat. No.
Lithium iron(III) oxide	$LiFeO_2$	95%	<1 µm	powder	442712-100G-A
Nickel zinc iron oxide	$NiZnFe_4O_4$	≥99% trace metals basis	particle size <100 nm BET)	nanopowder	641669-10G 641669-50G
Copper iron oxide	$CuFe_2O_4$	98.5% trace metals basis	particle size <100 nm BET)	nanopowder	641723-10G 641723-50G
Copper zinc iron oxide	$CuZnFe_4O_4$	98.5% trace metals basis	particle size <100 nm BET)	nanopowder	641650-10G 641650-50G
Yttrium iron oxide	$Y_3Fe_5O_{12}$	99.9% trace metals basis	particle size <100 nm BET)	nanopowder	634417-10G
Strontium ferrite	$SrFe_{12}O_{19}$	99.8% trace metals basis	particle size <50 nm XRD) particle size <100 nm BET)	crystalline (hexagonal phase) nanopowder	633836-5G
Strontium ferrite	$SrFe_{12}O_{19}$	99.5%	–325 mesh	powder	480371-5G 480371-25G
Barium ferrite	$BaFe_{12}O_{19}$	99.5% trace metals basis	particle size <100 nm BET)	nanopowder	637602-25G
Barium ferrite	$BaFe_{12}O_{19}$	98%	–325 mesh	powder	383295-250G 383295-1KG

Aluminates

Name	Formula	Purity	Dimensions	Physical Form	Cat. No.
Lithium aluminate	$LiAlO_2$	-	-	powder and chunks	336637-250G
Sodium aluminate	$NaAlO_2$	-	-	powder	13404-2.5KG-R 13404-5KG-R
Magnesium aluminate, spinel	$MgO{\cdot}Al_2O_3$	-	particle size <50 nm BET)	nanopowder	677396-5G
Copper aluminum oxide	$CuAl_2O_4$	98.5% trace metals basis	particle size <50 nm XRD) particle size <100 nm BET)	nanopowder	634301-25G
Lanthanum aluminum oxide	$LaAlO_3$	≥99.99% trace metals basis	10 × 10 × 0.5 mm	<100> single crystal substrate single side polished crystalline (rhombohedral at 25 °C (a = 5.357 Å, c = 13.22 Å); cubic at >435 °C (a = 3.821 Å))	634735-1EA
Aluminum cerium oxide	$AlCeO_3$	99% trace metals basis	particle size <50 nm BET)	nanopowder	637866-10G 637866-50G

High Temperature Boron-based Thermoelectric Materials

Takao Mori*

International Center for Materials Nanoachitectonics (MANA)
National Institute for Materials Science (NIMS)
Namiki 1-1, Tsukuba
Japan 305-0044
*Email: takao.mori@nims.go.jp

Introduction

The modern world is rapidly approaching the limits of classical energy reserves. Alternative sources of energy, such as the conversion of waste heat to electricity, offer potential and are an incentive to developing viable thermoelectric materials. In particular, materials that can function at high temperature and that withstand large temperature differences need to be developed for use in factories, power plants, incinerators, etc., as well as for reliable radiothermal generation of electricity in space applications.[1]

Boron-rich cluster compounds typically have melting points above 2200 K, and are therefore attractive materials for such purposes. They are also non-toxic, lightweight, and show remarkable stability in corrosive and acidic environments. Their synthesis is relatively straight forward, the addition of small amounts of carbon, nitrogen, or silicon to rare earth-boron systems (RE-B), to serve as bridging sites, results in the formation of novel boron cluster structures.[2]

Boron-rich cluster materials typically exhibit low intrinsic thermal conductivity (≤0.02 W cm^{-1} K^{-1}) even for single crystals, which gives them "built in" merit as thermoelectric materials.[2-4] The performance of thermoelectric materials is gauged by a dimensionless figure of merit ZT, where $ZT = \alpha^2\sigma T/\kappa$, and α is the Seebeck coefficient, σ is the electrical conductivity, and κ the thermal conductivity. Therefore, in a system with low κ it is possible to concentrate on maximizing the power factor, $P = \alpha^2\sigma$.

In this article, I focus on two novel boron-based compounds that have recently been discovered and that show promise in high temperature thermoelectric applications. The compounds are borosilicide, $REB_{44}Si_2$ (RE = rare earth) and homologous RE-B-C(N) borocarbides, including $REB_{17}CN$, $REB_{22}C_2N$, and $REB_{28.5}C_4$.

Emerging Boron-Based Materials and their Preparation

Boron is a versatile element, tending to form atomic networks based on clusters and 2D atomic nets in compounds. In this sense it is similar to carbon, which is able to form atomic network systems such as fullerenes, nanotubes, and graphite-related materials. Yet, the potential of boron in materials science is still largely untapped. Several striking properties of boron-containing compounds have recently been discovered, such as the superconductivity of MgB_2[5] (**Aldrich Prod. No. 553913**) and boron-doped diamonds,[6] the strong magnetic coupling in magnetically dilute insulators,[2] and the formation of a novel elemental structure of boron.[7]

Boron has one fewer electron than does carbon, which enables the formation of electron-deficient multi-atom networks. Such networks have a special affinity for the rare earth elements, which can supply electrons to the framework to stabilize and form novel structures (namely, new RE-B compounds), while the *f* electron shell is responsible for interesting properties, such as magnetism.[2,8]

From an application standpoint, the boron cluster framework provides a light robust "armor" that is acid and corrosion resistant, and can withstand very high temperatures. Additional electronic, magnetic, and other useful properties can be supplied by the metal atom from the "inside." As noted earlier, the addition of small amounts of such elements as carbon, nitrogen, or silicon further increases the number of novel boron-based compounds that can be created.[2] The crystal structure of the $REB_{44}Si_2$ compounds is shown in **Figure 1a**. It consists of five crystallographically independent B_{12} icosahedra (20-sided polyhedra) and one $B_{12}Si_3$ polyhedron. In the framework, the rare earth atoms form ladders in the direction of the c-axis, along which one of the B_{12} icosahedra also forms a chain.

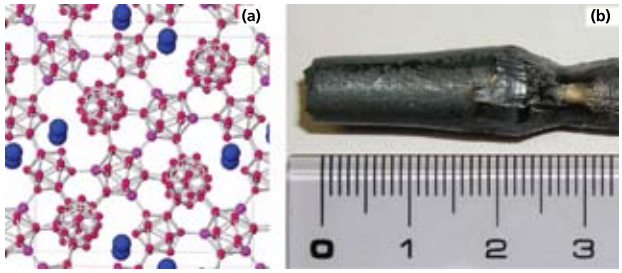

Figure 1. View of the (a) structure and (b) grown crystal of $REB_{44}Si_2$ (scale is cm).

Each of the rare earth-boron complexes $REB_{44}Si_2$, $REB_{17}CN$, $REB_{22}C_2N$, and $REB_{28.5}C_4$, can be synthesized in a similar way.[2] First, an appropriate rare earth oxide is reduced with boron (**Aldrich Prod. No. 266620**) upon heating under vacuum. Then, required amounts of elemental silicon (**Aldrich Prod. Nos. 633097, 343250, 267414**), carbon (**Aldrich Prod. Nos. 699632, 699624, 496596, 496553**), or boron nitride (**Aldrich Prod. No. 255475**) are added and heated again to produce the desired RE-B-X material. In the case of $REB_{44}Si_2$, it is possible to grow large crystals, as shown in **Figure 1b**.[9]

Borosilicides—New High Temperature p-Type Thermoelectric Materials

$REB_{44}Si_2$ compounds exhibit attractive high temperature thermoelectric properties.[10,11] Their Seebeck coefficients gradually increase with temperature, exceeding 200 μV K^{-1} above 1000 K (**Figure 2a**).[10] A low intrinsic thermal conductivity of about 0.02 W cm^{-1} K^{-1} has also been reported (**Figure 2b**).[11] Unlike most thermoelectric materials, the figure of merit of $REB_{44}Si_2$ shows a steep increase at temperatures beyond 1000 K, where an extrapolated value for ZT of about 0.2 can be estimated.

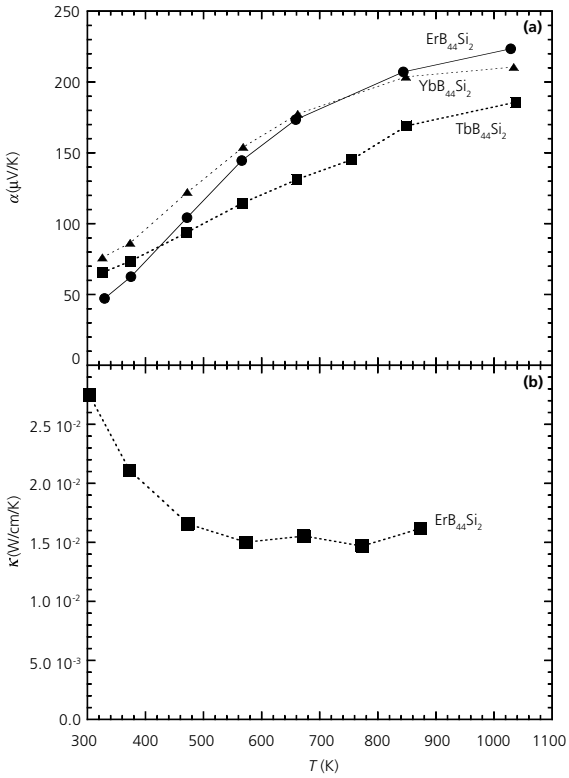

Figure 2. Temperature dependence of (a) Seebeck coefficient and (b) thermal conductivity of $REB_{44}Si_2$.

Considering that these compounds are not doped and are not composition optimized, their figure of merit and low intrinsic thermal conductivity indicate that they are good starting materials in the development of novel high temperature thermoelectric materials. It is noteworthy that the properties of boron carbide (**Aldrich Prod. No. 378119**), a classical thermoelectric material, can be significantly improved by controlling its carbon-boron composition.[12] Doping with transition metals is another way to efficiently modify the properties of $REB_{44}Si_2$. The transition metal atoms occupy voids between the boron clusters in the crystal lattice that, as indicated by our preliminary results, significantly increases the figure of merit of the doped material. Such doping efforts should be pursued further.

Control of the material's morphology is another avenue, which is being pursued since $REB_{44}Si_2$ compounds possess highly anisotropic crystal structures. The preparation of well-aligned materials can offer a powerful way to modify their thermoelectric properties.

Another advantage of $REB_{44}Si_2$ over boron carbide is its relatively low melting point (2200 K versus 2700 K), which allows easier processing. This, in conjunction with the properties previously mentioned, suggests that $REB_{44}Si_2$ can be an alternative to boron carbide as a high temperature p-type thermoelectric material, with the potential for further improvement through composition modification and doping.

RE-B-C(N) Borocarbides—Long Awaited n-Type Counterparts to Boron Carbide

The discovery of n-type RE-B-C(N) compounds is generating substantial interest due to their unique potential to serve as a high temperature thermoelectric counterpart to p-type boron carbide,[13,14] since typical thermoelectric applications require both p- and n-type legs.

RE-B-C(N) compounds have a layered structure along the c-axis with B_{12} icosahedra and C-B-C chain layers residing between the B_6 octahedral and the rare earth atomic layers (**Figure 3**). The number of interlayer B_{12} icosahedra and C-B-C chain layers increases successively along the series $REB_{17}CN$, $REB_{22}C_2N$, and $REB_{28.5}C_4$. As the number of C-B-C layers approaches infinity (that is, no rare earth-containing layers), the compound is analogous to boron carbide.

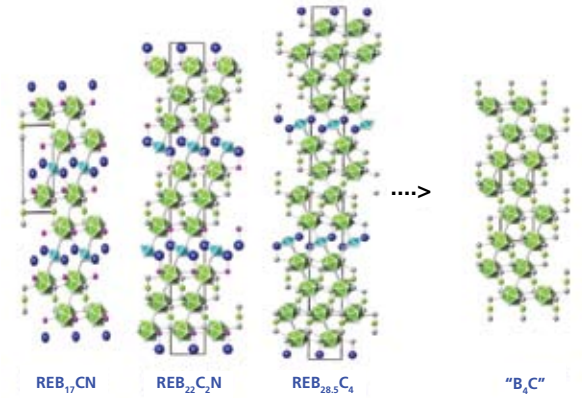

Figure 3. View of the structure of the homologous RE-B-C(N) compounds along the c-axis.

This similarity of RE-B-C(N) structural blocks to B_4C is the reason for considering them as compatible n-type counterparts to boron carbide, which has been established as an excellent p-type high temperature thermoelectric material.

One of the greatest challenges and opportunities for the RE-B-C(N) series is the development of an effective compaction procedure. Hot or cold pressing yields materials with densities of only about 50% of the theoretical value.[13] Initial attempts to use spark plasma sintering (SPS) yielded an improvement to about 70% of the theoretical value, which is still rather low.[14] The increase in density from 50% to 70% resulted in an increase in the figure of merit of close to two orders of magnitude. Therefore, the further development of a densification procedure is highly desirable.

An interesting way to control the morphology of RE-B-C(N) materials is by seeding them with a few percent of metallic borides (such as REB_6).[14] While seeding does not impact densities, the Seebeck coefficients and the thermal conductivities of doped materials, the resistivities of these materials are reduced by up to two orders of magnitude, offering an effective way to increase the material's figure of merit. Since the percent of doping is small, it is unlikely that a percolation effect, where the metallic boride particles create channels of high electrical conductivity, is the reason for the observed effect. As seen in **Figure 4,** the metal-seeded sample has larger grain sizes than the undoped sample, indicating that the addition of metallic borides promotes grain growth in RE-B-C(N). We note that compared with conventional thermoelectric materials, in which it is usually preferred to inhibit grain growth in order to depress thermal conductivity, boron cluster compounds possess low intrinsic thermal conductivity, and therefore grain growth is beneficial. Thus, the seeding provides an efficient tool to control the morphology of the samples and to improve their thermoelectric properties.

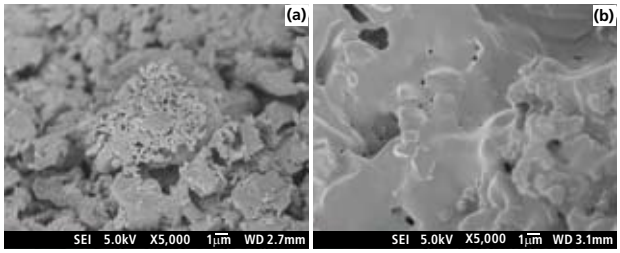

Figure 4. SEM microstructures of (a) $YB_{22}C_2N$ and (b) $ErB_{22}C_2N$:ErB_4.

RE-B-C(N) borocarbides demonstrate high anisotropy of the crystal structure (**Figure 3**), making further control of the nano- and microstructure of the samples a powerful tool for the enhancement, or tuning, of their thermoelectric properties. Further investigations should continue into the processing and densification of this system. It is hoped that this system will be a viable n-type counterpart to boron carbide.

Summary

Boron-based compounds are promising systems due to their high temperature thermoelectric properties. They are high temperature materials (typically possessing melting points above 2200 K), non-toxic, lightweight, and show remarkable stability in corrosive or acidic conditions. Two novel boron-based compounds are especially promising. $REB_{44}Si_2$ is a p-type high temperature compound that retains the low thermal conductivity exhibited by well known boron cluster compounds, such as REB_{66}, while improving the electrical properties and thermoelectric figure of merit. $REB_{44}Si_2$ can be more readily melted and therefore might be advantageous in processing when compared to boron carbide. The rare earth borocarbides, $REB_{17}CN$, $REB_{22}C_2N$, and $REB_{28.5}C_4$, represent the first instance of intrinsic n-type behavior in boron cluster compounds, and are interesting as a highly compatible counterpart to boron carbide. Both compound systems have recently been discovered and further development should prove rewarding, since the benefits of finding materials able to viably convert high temperature waste heat to electricity are immense.

Research into the optimization and processing of these compounds has just begun. Composition control, carbon doping, and doping the voids of the clusters should greatly enhance the materials' thermoelectric properties. Optimizing densification processes for the borocarbides and ways to control the nano- and microstructure of both anisotropic compounds will be valuable tools in the further development of materials for high temperature thermoelectric applications.

References:

(1) *Chemistry, Physics and Materials Science of Thermoelectric Materials: Beyond Bismuth Telluride,* Kanatzidis, M..G.; Mahanti, S.D.; Hogan, T.P., Ed.; Kluwer: New York, 2003.
(2) Mori, T. *Handbook on the Physics and Chemistry of Rare Earths,* Gschneidner Jr, K.A.; Bunzli, J.C.; Pecharsky, V., Eds.; Elsevier:Amsterdam, 2008; Vol. 38; p 105.
(3) Mori, T.; Martin, J.; Nolas, G. *J. Appl. Phys.* **2007**, *102*, 073510.
(4) Cahill, D.G.; Fischer, H.E.; Watson, S.K.; Pohl, R.O.; Slack, G.A. *Phys. Rev.* B, **1989**, *40,* 3254.
(5) Nagamatsu, J.; Nakagawa, N.; Muranaka, T.; Zenitani, Y.; Akimitsu, J.; *Nature*, **2001**, *410*, 63.
(6) Ekimov, E. A.; Sidorov V.A.; Bauer E.D.; Mel'nik, N.N.; Curro N.J.; Thompson J.D.; Stishov, S.M.; *Nature*, **2004**, *428*, 542
(7) Oganov, A.R.; Chen, J.; Gatti, C.; Ma, Y.; Glass, C.W.; Liu, Z.; Yu, T.; Kurakevych, O.O.; Solozhenko, V.L.; *Nature* **2009**, *457*, 863.
(8) Mori, T.; Tanaka, T. *J. Phys. Soc. Jpn.*, **1999**, *68,* 2033.
(9) Mori, T. *Z. Krist.*, **2006**, *221,* 464.
(10) Mori, T. *J. Appl. Phys.*, **2005**, 97, 093703.
(11) Mori, T. *Physica B,* **2006**, *383,* 120.
(12) Wood, C.; Emin, D. *Phys. Rev. B,* **1984**, *29*, 4582.
(13) Mori, T.; Nishimura, T. *J. Solid State Chem.*, **2006**, *179,* 2908.
(14) Mori, T.; Nishimura, T.; Yamaura, K.; Takayama-Muromachi, E. *J. Appl. Phys.* **2007**, *101,* 093714.

Borides

For a complete list of metals, oxides, ceramics and related materials, please visit ***sigma-aldrich.com/ceramics***

Name	Formula	Purity	Dimensions	Physical Form	Cat. No.
Magnesium boride	MgB_2	≥96%	–325 mesh	powder	553913-5G 553913-25G
Aluminum diboride	AlB_2	-	–325 mesh	powder	399612-5G
Aluminum dodecaboride	AlB_{12}	-	–325 mesh	powder	399604-5G
Calcium hexaboride	CaB_6	99.5%	–200 mesh	powder	394785-10G
Titanium boride	TiB_2	-	<10 μm	powder	336289-50G
Chromium diboride	CrB_2	≥99%	–325 mesh	powder	336750-50G
Cobalt boride, mixture of 2:1 and 3:1	-	99%	–10 mesh	powder	336777-5G 336777-25G
Nickel boride	Ni_2B	99%	–30 mesh	powder	372633-10G 372633-100G
Nickel boride	NiB	99% trace metals basis	–325 mesh	powder	709174-10G
Niobium monoboride	NbB	99.5%	–325 mesh	powder	399515-25G
Niobium diboride	NbB_2	-	–325 mesh	powder	399507-10G
Molybdenum boride	MoB	99.5% trace metals basis	–325 mesh	powder	709182-10G
Lanthanum boride	LaB_6	99.5% trace metals basis	–325 mesh	powder	709190-5G
Lanthanum hexaboride	LaB_6	99%	10 μm	powder	241857-25G
Gadolinium boride	GdB_6	99.5% trace metals basis	–325 mesh	powder	709212-10G
Hafnium boride	HfB_2	99.5% trace metals basis	–325 mesh	powder	709204-10G
Tantalum boride (1:1)	TaB	99.5%	–325 mesh	powder	336165-5G
Tantalum boride (1:2)	TaB_2	99.5%	–325 mesh	powder	336173-5G
Tungsten boride	WB	≥97.0%, gravimetric	-	powder	10497-25G

Nitrides

Name	Formula	Purity	Dimensions	Physical Form	Cat. No.
Lithium nitride	Li_3N	≥99.9%	–80 mesh	powder	399558-5G 399558-10G 399558-25G
Boron nitride	BN	98%	~1 µm	powder	255475-10G 255475-50G 255475-250G
Magnesium nitride	Mg_3N_2	≥99.5% trace metals basis	–325 mesh	cubic phase powder	415111-10G 415111-50G
Aluminum nitride	AlN	≥98%	10 µm	powder	241903-50G 241903-250G
Aluminum nitride	AlN	≥98.5%	particle size <100 nm	nanopowder	593044-10G 593044-50G
Silicon nitride	Si_3N_4	-	–325 mesh	predominantly α-phase powder	325171-50G 325171-250G
Silicon nitride	Si_3N_4	≥98.5% trace metals basis	particle size <50 nm spherical)	nanopowder	636703-25G 636703-100G
Silicon nitride	Si_3N_4	≥98% trace metals basis	particle size <50 nm BET)	nanopowder	634581-5G 634581-25G
Silicon nitride	Si_3N_4	≥99.9% trace metals basis	<1 µm	powder	334103-25G 334103-100G
Silicon nitride	Si_3N_4	-	–325 mesh	predominantly β-phase powder	248622-100G 248622-500G
Calcium nitride	Ca_3N_2	95%	–200 mesh	powder	415103-25G 415103-100G
Titanium nitride	TiN	-	<3 µm	powder	595063-25G 595063-100G
Titanium carbonitride (7:3)	$TiC_{0.7}N_{0.3}$	≥97% trace metals basis	particle size <150 nm	nanopowder	636940-25G
Titanium carbonitride	TiCN	≥97% trace metals basis	particle size <150 nm spherical)	nanopowder	636959-25G 636959-100G
Gallium nitride	GaN	≥99.99% trace metals basis	-	powder	481769-10G 481769-50G
Germanium(III) nitride	Ge_3N_4	≥99.99% trace metals basis	-	powder	447552-5G
Zirconium nitride	ZrN	≥99% trace metals basis	-	powder	594962-10G 594962-50G
Indium(III) nitride	InN	99.9% trace metals basis	100 mesh	powder	490628-1G 490628-5G

Rare Earth Oxides

Name	Formula	Purity	Physical Form	Cat. No.
Lanthanum(III) oxide	La_2O_3	99.999% trace metals basis	powder	203556-100G 203556-500G
Lanthanum(III) oxide	La_2O_3	99.99% trace metals basis	powder	199923-100G 199923-500G
Lanthanum(III) oxide	La_2O_3	≥99.9%	powder	L4000-100G L4000-250G L4000-500G L4000-1KG
Cerium(IV) oxide	CeO_2	99.995% trace metals basis	powder	202975-10G 202975-50G
Cerium(IV) oxide	CeO_2	>99.95% trace metals basis	nanopowder	700290-25G 700290-100G
Cerium(IV) oxide	CeO_2	-	nanopowder	544841-5G 544841-25G

Name	Formula	Purity	Physical Form	Cat. No.
Praseodymium(III) oxide	Pr_2O_3	99.9% trace metals basis	powder	558249-10G 558249-50G
Praseodymium(III,IV) oxide	Pr_6O_{11}	99.999% trace metals basis	powder	204145-2G 204145-10G
Praseodymium(III,IV) oxide	Pr_6O_{11}	99.9% trace metals basis	powder	205176-50G 205176-250G
Neodymium(III) oxide	Nd_2O_3	99.99% trace metals basis	powder	203858-10G 203858-50G
Neodymium(III) oxide	Nd_2O_3	99.9% trace metals basis	powder	228656-25G 228656-100G
Neodymium(III) oxide	Nd_2O_3	99.9% trace metals basis	nanopowder	634611-5G 634611-50G
Samarium(III) oxide	Sm_2O_3	99.999% trace metals basis	powder	394394-5G 394394-25G
Samarium(III) oxide	Sm_2O_3	99.99% trace metals basis	powder	392537-5G 392537-25G
Samarium(III) oxide	Sm_2O_3	99.9% trace metals basis	powder	228672-10G 228672-100G
Europium(III) oxide	Eu_2O_3	99.999% trace metals basis	powder and chunks	323543-1G 323543-5G
Europium(III) oxide	Eu_2O_3	99.99% trace metals basis	powder	203262-5G 203262-25G
Europium(III) oxide	Eu_2O_3	99.9% trace metals basis	powder	289221-5G 289221-25G
Gadolinium(III) oxide	Gd_2O_3	≥99.99% trace metals basis	powder	203297-5G
Gadolinium(III) oxide	Gd_2O_3	99.9% trace metals basis	powder	278513-25G 278513-100G
Terbium(III) oxide	Tb_2O_3	99.99% trace metals basis	powder	590509-2G 590509-10G
Terbium(III,IV) oxide	Tb_4O_7	99.999% trace metals basis	powder	204579-2G
Terbium(III,IV) oxide	Tb_4O_7	99.9% trace metals basis	powder	253952-10G
Dysprosium(III) oxide	Dy_2O_3	≥99.99% trace metals basis	powder	203181-5G 203181-25G
Dysprosium(III) oxide	Dy_2O_3	99.9% trace metals basis	powder	289264-25G 289264-100G
Holmium(III) oxide	Ho_2O_3	99.999% trace metals basis	powder	229679-1G 229679-10G
Holmium(III) oxide	Ho_2O_3	≥99.9% (rare earth content, expressed as Ho_2O_3)	powder	H9750-10G H9750-50G
Erbium(III) oxide	Er_2O_3	≥99.99% trace metals basis	powder	203238-5G 203238-25G
Erbium(III) oxide	Er_2O_3	99.9% trace metals basis	powder	289248-25G
Thulium(III) oxide	Tm_2O_3	99.99% trace metals basis	powder	204676-1G
Thulium(III) oxide	Tm_2O_3	99.9% trace metals basis	powder	289167-1G 289167-5G
Ytterbium(III) oxide	Yb_2O_3	99.99% trace metals basis	powder	204889-10G
Ytterbium(III) oxide	Yb_2O_3	99.9% trace metals basis	powder	246999-10G 246999-50G
Lutetium (III) oxide	Lu_2O_3	99.99% trace metals basis	powder	203661-1G 203661-5G
Lutetium (III) oxide	Lu_2O_3	99.9% trace metals basis	powder	289191-1G 289191-5G

Ultra Pure Metal Oxide Powders For High Technology Applications

Our manufacturing facility in Urbana, Illinois, USA is a Materials Chemistry Center of Excellence for the production of very high purity oxides used in a wide variety of applications ranging from high technology to ceramics to dental. Ultra-pure oxides are provided for numerous elements including alkaline earth, transition and rare earth metals. Our capabilities include several specialized synthesis and purification techniques, resulting in our ability to consistently supply oxides of trace metal purities ranging from 3N (99.9%) to 5N (99.999%). Several of our ultra-pure oxide products are offered in discrete particle size ranges for custom applications.

Please contact us today for your specific requirements: matsci@sial.com

Cat. No.	Material	Purity
394394	Samarium (III) oxide	99.999%
204951	Zinc oxide	99.999%
202975	Cerium (IV) oxide	99.995%
450804	Copper (II) oxide	99.995%
590509	Terbium (III) oxide	99.99%
463744	Vanadium (III) oxide	99.99%
554847	Barium oxide	99.99%
675644	Chromium (VI) oxide	99.99%
566284	Copper (I) oxide	99.99%
203238	Erbium (III) oxide	99.99%
215066	Gallium (III) oxide	99.99%
518158	Iron (II/III) oxide	99.99%
203815	Molybdenum (VI) oxide	99.99%
203394	Hafnium oxide	99.95%
415138	Strontium oxide	99.9%

Silicon Carbide: The Return of an Old Friend

Nicholas G. Wright* and Alton B. Horsfall

School of Electrical, Electronic and Computer Engineering
Newcastle University
Newcastle upon Tyne, UK
*Email: n.g.wright@ncl.ac.uk

Introduction

In recent years silicon carbide, SiC, has re-emerged as a vital technological material that is crucial in many materials and engineering applications. Interestingly, SiC is one of the few minerals that were first created synthetically and subsequently discovered in nature. It was first artificially synthesized in 1891 by Edward Acheson as a result of unexpectedly discovering small black crystals of SiC in an electrically heated melt of carbon and alumina.[1] The subsequent refinement of this technique (the so-called Acheson process) led to the commercial production of large volumes of small SiC crystals (ground into powder form) for use as an industrial abrasive.[2] In 1905, silicon carbide was observed in its natural form by the Nobel-prize-winning chemist Henri Moissan in Diablo Canyon, Arizona. The transparent mineral, now known as moissanite, is almost as brilliant and as hard as diamond, and is therefore often used as a gemstone. To date, no large natural deposits of SiC have ever been found in nature so all SiC used today is synthetic.

In the present day, SiC is one of the most widely used materials that plays a critical role in industries such as: aerospace, electronics, industrial furnaces and wear-resistant mechanical parts among others. Although SiC is widely used in electronics and other high technology applications, the metallurgical, abrasive, and refractory industries are dominating by volume.

Crystal Structure

Silicon carbide has a layered crystal structure which occurs in a number of different forms or polytypes. Composed of carbon and silicon, in equal amounts, each atom is bonded to four atoms of the opposite type in a tetrahedral bonding configuration. There are three possible arrangements of atoms in a layer of SiC crystal known as the A, B and C positions, and each polytype has the same layers but a different stacking sequence (**see Figure 1**).[3] As a given layer may be stacked on top of another in a variety of orientations (with both lateral translations and rotations being feasible energetically), silicon carbide may occur in a wide variety of stacking sequences—each unique stacking sequence generating a different polytype (e.g., cubic, hexagonal and rhombohedral structures can all occur). The hexagonal and rhombohedral structures, designated as the α-form (noncubic), may crystallize in a large number of polytypes whilst, to date, only one form of cubic structure (designated as the β-form) has been recorded. Designation[4] is by the number of layers in the sequence, followed by H, R, or C to indicate whether the type belongs to the hexagonal, rhombohedral, or cubic class. To date, over 215 polytypes have been recorded—although only a limited number are of interest technologically (principally the 4H and 6H hexagonal plus the 3C cubic forms).[5]

This interest is driven by the commercial availability of substrates and the low mobility anisotropy (difference in carrier mobility with crystallographic direction) for these polytypes.

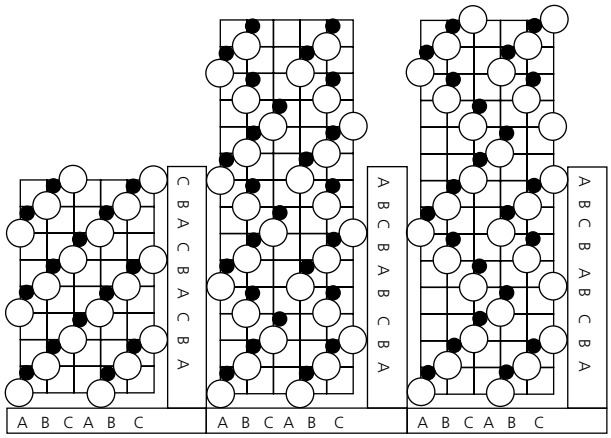

Figure 1. Stacking sequences of the Crystal structures of (a) 3C SiC, (b) 4H SiC, and (c) 6H SiC.

The term "silicon carbide" is commonly used to describe a range of materials that are in fact quite distinct. Mechanical engineers may use it to describe ceramics which are fabricated from relatively impure SiC crystallites bonded together with various binders under temperature and/or pressure, while electrical engineers may use the term to describe high purity single crystal wafers of SiC.

Applications Based on Mechanical Properties

All forms of silicon carbide are well known as hard materials occupying a relative position on Mohs' scale between alumina at 9 and diamond at 10.[6] Because of its high thermal conductivity and low thermal expansion, silicon carbide is very resistant to thermal shock as compared to other refractory materials.[6] Until the recent emergence of silicon carbide as a significant material for electronics, the mechanical properties of SiC-ceramics were the dominant commercial interest.

The formation of SiC powder is an essential pre-requisite to the manufacturing of many types of ceramic articles, which are subsequently obtained by shaping the manufactured silicon carbide powder. SiC powders with variable purity levels, crystal structures, particle sizes, shapes, and distributions can be prepared via several routes. Methods that have been examined include: growth by sublimation carbothermic reduction (the Acheson Process), conversion from polymers and gas phase chemical reactions.

Although brittle in nature, silicon carbide ceramics are leading materials for rotating and static components in many mechanical applications. They are characterized by low fracture toughness and limited strain-to-failure as compared to metals. The strength of a silicon carbide ceramic component is generally determined by pre-existing flaws introduced into the material during processing. The type, size, shape, and location of the flaws vary considerably and, consequently, so does the strength. Silicon carbide ceramics made by different techniques also have quite distinct mechanical properties. For example, sintered silicon carbide retains its strength at elevated temperatures and shows excellent time-dependent properties such as creep and slow crack growth resistance. In contrast, reaction-bonded SiC, because of the presence of free silicon in its microstructure, exhibits slightly inferior elevated temperature properties.[7]

The extreme hardness of silicon carbide leads to its use as a coating when wear resistance is important, such as brake linings and electrical contacts, and in non-slip applications such as floor or stair treads, terrazzo tile, deck-paint formulations, and road surfaces. SiC is also commonly used in mechanical seals found in pumps, compressors, and agitators in a wide variety of demanding environments including highly corrosive ones. Silicon carbide is harder, yet more brittle, than other abrasives such as aluminum oxide (**Aldrich Prod. Nos. 202606, 342750**). Because the grains fracture readily and maintain a sharp cutting action, silicon carbide abrasives are usually used for grinding hard, low tensile-strength materials such as chilled iron, marble, and granite, and materials that need sharp cutting action such as fiber, rubber, leather, or copper. Silicon carbide is also used in a loose form for lapping; mixed with other materials to form abrasive pastes, or used with cloth backings to form abrasive sheets, disks, or belts.[6]

Applications Based on Electronic and Optical Properties

In recent years, SiC has emerged as a promising material for electronics.[8,9] Silicon carbide is considered a wide bandgap material since the electronic bandgaps of the different polytypes range from 2.4eV to 3.3eV (c.f., silicon with a bandgap of 1.1eV).[10] In some respects, such a wide range of bandgaps is unexpected—particularly when the crystal structures of the polytypes differ only in the stacking sequence of otherwise identical bilayers (see Figure 1). Research in recent years has enabled the development of processing techniques that enable the material properties of silicon carbide to be modified successfully for electronics, in particular power electronics and sensors.[11] In addition, silicon carbide is commonly used as a substrate material for light emitting diodes where it acts as a foundation on which optically active layers can be grown. This growth utilizes the close lattice match between 6H SiC, gallium nitride and the high thermal conductivity of SiC to remove the heat generated in the LED.

One application where silicon carbide is making a big impact is gas sensors.[12] Its wide band gap gives it very low intrinsic carrier concentration, making sensing possible in very hot gases, such as the pollutants released in combustion engines and the sulphurous emissions from volcanic vents. A typical silicon-carbide gas sensor is about 100 μm across and a fraction of a millimeter thick, and are typically based on a capacitor (MIS structure) with a catalytic contact as shown in **Figure 2**.[13] The dielectric layer allows these devices to operate at temperatures in excess of 900°C,[14] by separating the metal from the silicon carbide. In this technology, dielectric layers are typically metal oxide materials such as TiO_2, or HfO_2 (**Aldrich Prod. Nos. 203394 and 202118**), which can be deposited in a variety of manners—including in-situ oxidation of metal layers or more sophisticated techniques such as Atomic Later Deposition with relevant precursors.[15] When the metal surface is exposed to a gas mixture, it speeds up the breakdown of the gas molecules, releasing ions that modify the electrical properties of the device. For hydrogen and hydrogen containing molecules, the hydrogen atoms can diffuse easily through thick or dense catalytic contacts to form the charged layer following decomposition of the gas molecule that occurs at temperatures above 150 °C in the sub-millisecond time scale.[16] The response of the sensor can be measured via a number of methods including: capacitance shift, voltage shift required to maintain capacitance, or the leakage current through the dielectric layers. The high electrical response speed makes silicon carbide sensors suitable for the detection of gas species in rapidly varying environments, such as close to the manifold region in car exhausts,[17] unlike conventional ceramic based sensors, which have a response time in the region of 10 seconds under these conditions.[18]

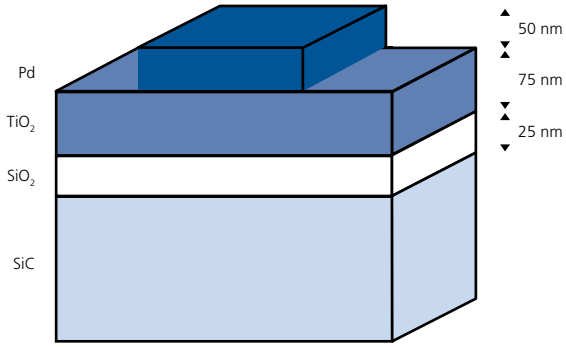

Figure 2. Cross-section of a SiC gas sensor. The SiO_2 layer is used to reduce the leakage current at high operating temperatures, due to the high band offsets and to reduce the defect density at the SiC/SiO_2 interface (Figure reproduced with permission from ref. 14. © 2007 IEEE). The SiC comprises a heavily doped substrate, which is typically 350μm thick and a lightly doped epilayer of a few μm thickness.

Disentangling the effects of the different gases to determine the composition of a mixture is not easy. At temperatures above 600 °C the gas species dissociate completely at the metal surface, making it impossible to identify individual gases. For example, molecules of methane and ethane produce four and six hydrogen ions, respectively, when completely dissociated. This means that we cannot distinguish between a given concentration of methane and two-thirds of that concentration of ethane since both produce the same number of hydrogen ions. Below a temperature of 150 °C, the dissociation of gas species at the catalytic surface does not occur and the sensors do not respond to the gas at all. Between 150 °C and 600 °C the gas species dissociate only partially, and an array of sensors, with different characteristics to uniquely identify the gases present, can be used. For example, palladium is more sensitive to hydrogen and platinum to ammonia, so using one sensor with each metal allows these gases to be distinguished. Complex computer algorithms such as "Gaussian mixed modes" and "primary component analysis" are then used to decompose the measured electrical response of the devices into the known responses to each individual gas. As a consequence of these effects, the sensitivity of such devices to different gases does vary with temperature, although calibration can be used (as with all sensors) to produce accurate and reproducible readings (**see Figure 3**).

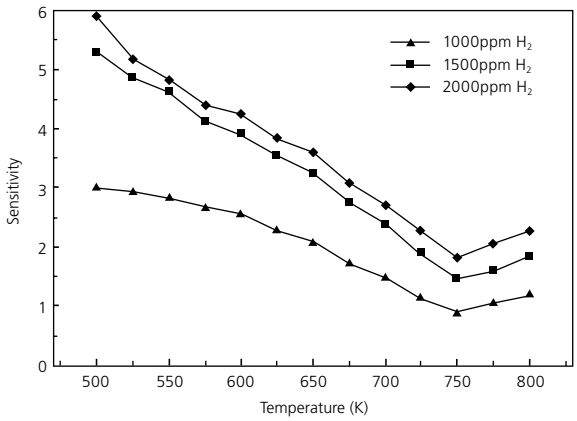

Figure 3. Variation in sensitivity with temperature for a typical SiC gas sensor (Figure reproduced with permission from ref. 14. © 2007 IEEE).

Conclusion

Silicon carbide has emerged as a crucial technological material in recent years; not just for mechanical use, but also as an electronic and optical material. Its excellent material properties and the emergence of underpinning material processing techniques promise a bright future for silicon carbide in many areas of science and engineering.

References:

(1) Acheson, E.G. *J. Franklin Inst.* **1893**, *136*, 279.
(2) Acheson, E.G. To the Carborundum Co. U.S. Patent 492,767. Feb. 28, 1893.
(3) Shaffer, P.T.B. *Acta Cryst.* **1969**, *B25*, 477.
(4) Ramsdell, L.S. *Am. Mineral.* **1947**, *32*, 64.
(5) *Properties Of Silicon Carbide*, Harris, G.L., Ed.; INSPEC: London, 1995.
(6) Silicon Carbide. *Kirk-Othmer Encyclopedia Of Chemical Technology*, 5th ed.; Wiley: New York, 2006; Vol 22.
(7) Srinivasan, M. *Structural Ceramics, Treatise On Materials Science And Technology*; Wachtman, Jr., J.B., Ed.; Academic Press, Inc.: New York, 1989; Vol. 29.
(8) Baliga, B.J. *Silicon Carbide Power Devices*, World Scientific Press: Singapore, 2006.
(9) *Silicon Carbide: Recent Major Advances*; Choyke, W.J.; Matsunami, H.; Pensl, G., Eds.; Springer: Berlin, 2006.
(10) Goldberg, Y.; Levinshtein, M.; Rumyantsev, S. *Properties Of Advanced Semiconductor Materials;* Levinshtein, M.; Rumyantsev, S.; Shur, M., Eds.; Wiley: New York, 2001.
(11) *Silicon Carbide: Materials, Processing And Devices*; Feng, Z.C.; Zhao, J.H., Eds.; Taylor And Francis: New York, 2006.
(12) Wright, N.G.; Horsfall, A. B. *Journal Of Physics D- Applied Physics*, **2007,** *40*, 6345.
(13) Weng, M.H.; Mahapatra, R.; Wright, N.G.; Horsfall, A.B. *Meas. Sci. Technol,*. **2008**, *19,* 024002.
(14) Weng, M.H.; Mahapatra, R.; Horsfall, A.B.; Wright, N.G. *IEEE Sensors Journal*, **2007**, *7*, 1395.
(15) Sigma-Aldrich Catalog (2009-2010).
(16) Nakagomi, S.; Tobias, P.; Baranzahi, A.; Lundstrom, I.; Maretnsson, P.; Spetz, A.L. *Sensors And Actuators B*, **1997**, *45*, 183.
(17) Baranzahi, A.; Spetz, A. L.; Glavmo, M.; Nytomt, J.; Lundstrom, I. *Proceedings, 8th International Conference on Solid-state Sensors and Actuators, and Eurosensors IX, Stockholm Sweden*, **1995**, 741.
(18) Xiong, W.; Kale, G. *Sensors And Actuators B*, **2005**, *114*, 101.

Silicon Carbide

For a complete list of metals, oxides, ceramics and related materials, please visit ***sigma-aldrich.com/ceramics***

Name	Formula	Purity	Dimensions	Physical Form	Cat. No.
Silicon carbide	SiC	>95% by XRD	particle size 200 - 450 mesh	powder	378097-250G 378097-1KG
Silicon carbide	SiC	≥97.5%	particle size –400 mesh	hexagonal phase powder	357391-250G 357391-1KG
Silicon carbide	SiC	>95% by XRD	particle size <100 nm	nanopowder	594911-100G 594911-250G

Metal Carbides

Name	Formula	Purity	Dimensions	Physical Form	Cat. No.
Aluminum carbide	Al_4C_3	99%	–325 mesh	cubic phase powder	241873-25G 241873-100G
Tungsten(IV) carbide	WC	99%	10 µm	powder	241881-100G
Calcium carbide	CaC_2	~80%	thickness <10 mm (typically)	pieces	270296-500G 270296-2KG
Calcium carbide	CaC_2	≥75%, gas-volumetric	particle size 0.3 - 1 mm	pieces	21039-100G-F 21039-1KG-F
Tantalum(IV) carbide	TaC	99%	≤5 µm	powder	280801-10G
Titanium(IV) carbide	TiC	98%	–325 mesh	powder	307807-100G 307807-500G
Zirconium(IV) carbide	ZrC	99%	5 µm	cubic phase powder	336351-50G 336351-250G
Boron carbide	CB_4	98%	10 µm	powder	378119-50G
Boron carbide	CB_4	98%	–200 mesh	powder	378100-100G 378100-500G
Molybdenum carbide	Mo_2C	99.5%	–325 mesh	powder	399531-50G
Chromium carbide	Cr_3C_2	99.5%	–325 mesh	powder	402680-50G 402680-250G
Hafnium(IV) carbide	HfC	-	particle size <1.25 µm	powder	594636-25G
Titanium(IV) carbide	TiC	≥95%	<4 µm	powder	594849-25G 594849-100G
Titanium(IV) carbide	TiC	95%	particle size <200 nm BET)	nanopowder	636967-25G 636967-100G 636967-250G

Silicides

Name	Formula	Purity	Dimensions	Physical Form	Cat. No.
Magnesium silicide	Mg_2Si	≥99% trace metals basis	–20 mesh	powder	343196-25G
Molybdenum disilicide	$MoSi_2$	≥99% trace metals basis	-	powder	243647-250G
Tungsten silicide	WSi_2	99.5%	–325 mesh	powder	399442-10G
Calcium silicide	$CaSi_2$	-	-	powder	21240-250G-F 21240-1KG-F

Interactive Periodic Table

Ceramics and Related Materials

ALDRICH Chemistry

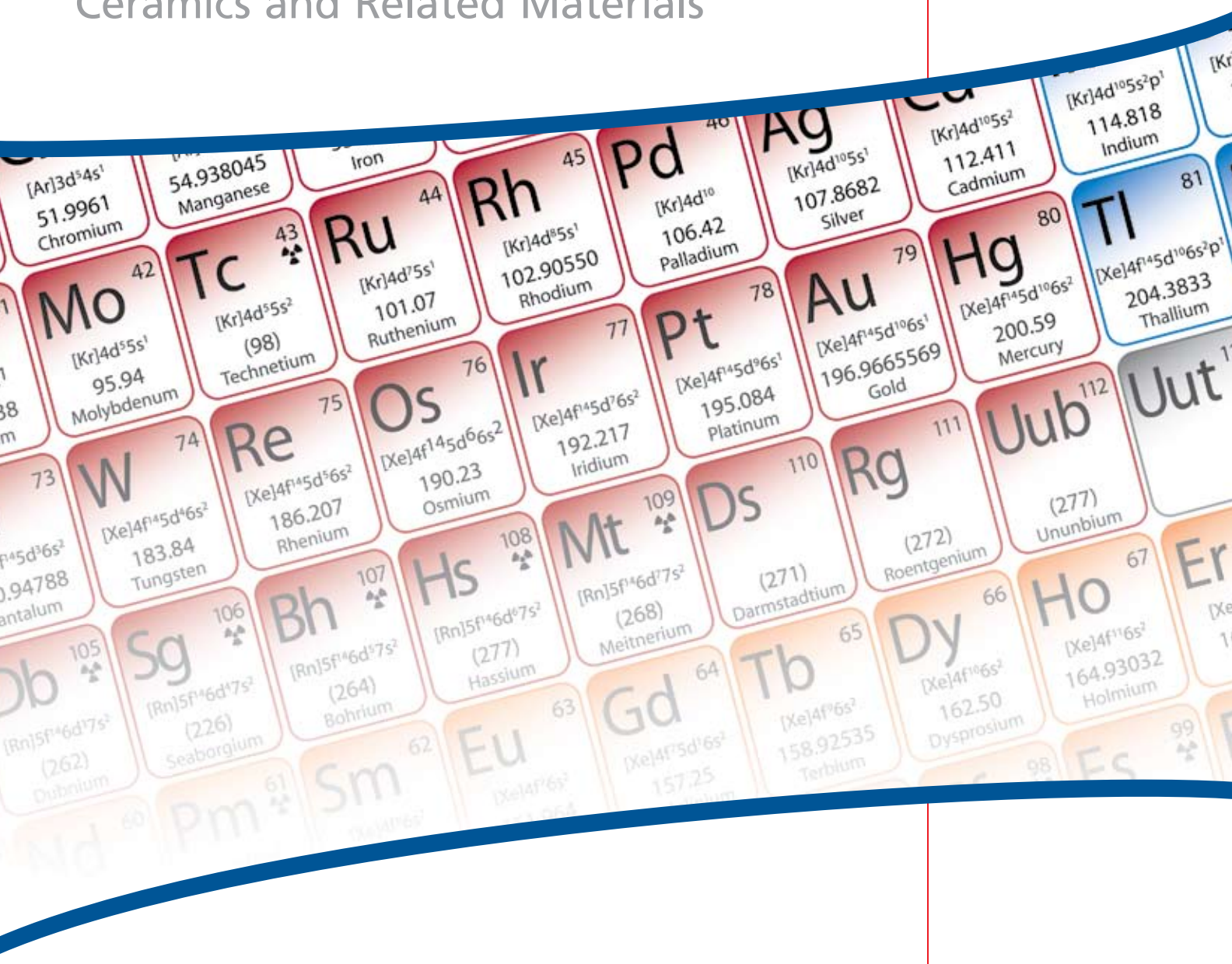

An easy way to navigate through Aldrich Ceramic Materials on the Web.

- Aluminates
- Arsenides
- Borides
- Carbides
- Ferrites
- Niobates
- Nitrides
- Phosphides
- Silicides
- Titanates
- Tungstanates
- Zirconates

also Metals, Salts, Organometallic Precursors and more.

Visit the Interactive Periodic Table at *sigma-aldrich.com/periodic*

Mesoporous Oxides and Their Applications to Hydrogen Storage



Arlon J. Hunt[1]*, Karl Gross[2]*, Samuel S. Mao[1]*

[1]Lawrence Berkeley National Laboratory
1 Cyclotron Road, Berkeley, CA 94720
[2]H2 Technology Consulting LLC
33902 Juliet Circle
Fremont, CA 94555
*E-mail: ajhunt@lbl.gov, kgross@h2techconsulting.com, ssmao@newton.berkeley.edu

Introduction

Solid-state hydrogen storage is attractive from a technological point of view, but has encountered tremendous challenges in terms of practical storage capacity and kinetics.[1-3] Hydrogen sorption, whether it is chemisorption of dissociated atomic hydrogen or van der Waals weak physisorption of molecular hydrogen, depends strongly on material-specific surface interactions. High-surface area carbon materials and metal hydrides (including complex hydrides) represent two distinctive categories of candidate materials for solid-state hydrogen storage and have been the focus of intensive research.

More recently, metal-organic frameworks[4,5] have emerged as an important class of physisorption hydrogen storage materials due to the possibility of designing them with functionalized porous structures as well as their low density and high specific surface area. On the other hand, reversible chemisorption materials, such as metal hydrides, exhibit high formula hydrogen storage capacities. However, their practical use is often limited by high thermodynamic stability (e.g., MgH_2) or poor reaction kinetics (e.g., Alanates). New approaches that simultaneously address reaction chemistry, compositional modifications, and reactant heat and mass transport are needed to overcome these barriers to realizing practical hydrogen storage. To address these issues, we base our approach on low density, metal oxide based, ceramic materials produced using sol-gel processing, then modifying those structures using a variety of methods to form modified active oxide networks.

Low Density Mesoporous Oxides

Mesoporous materials, such as aerogels, offer several advantages over other materials due to their large surface area (over 1000 m^2/gm), open porosity (80 to 99.9% porous), small pore sizes (typically peaking at 10-20 nm), and the ability to coat the surface of the mesoporous structure with one or more compounds. These materials are made using sol-gel processing followed by drying using solvent extraction. If the solvent extraction is carried out using supercritical processing the resultant material is called an aerogel. Aerogels were discovered by Kistler in 1931.[6] Kistler's pioneering work centered on demonstrating that a "gel" is made up of a solid framework containing the liquid from which it was formed. Because drying the gels in air causes them to shrink considerably and fracture into many pieces he surmised that surface tension forces were collapsing the submicroscopic pores. To avoid the surface tension forces he first substituted ethanol for the liquid in the gel, then raised the temperature and pressure above the critical point of ethanol (243.1°C and 63.1 bar) to eliminate the surface tension. At this point he slowly lowered the pressure, allowing the fluid to expand and leave the gel. He named the resulting material aerogel because it contained air rather than liquid. Alternatively, air dried gels are typically much denser and are termed xerogels.

Aerogels have been proposed for a wide variety of applications because of their unique properties. They are the lightest solid materials, with up to 99.7% porosity, transparent and excellent solid thermal insulators. In addition, aerogels have the lowest sound conductivity of any material (less than 100 m/sec, the sound velocity in air is 343 m/sec). They have been used to prepare Cherenkov counters, superinsulating windows, solar collector covers, refrigerators, spacecraft, water heaters and pipe insulation. Unique shock wave characteristics of ceramic aerogels led to their use as space dust collectors in earth orbit and the Stardust mission to the comet Wilde II which returned the first meteoric dust to earth. Aerogels have also been tested as high performance electrical insulation because of their high breakdown voltage, as catalysts due to their high surface area, for gas filters because of their fine pore sizes, for vapor phase pumps driven by temperature differences and aided by their hydrophilic nature, toxic cleanup materials, elements of acoustic devices and even safe insecticides.

An open pore aerogel structure may be made from many inorganic oxides, carbon, or polymers. In fact, aerogel mesoporous materials may be thought of as a "three dimensional canvas" that can be "painted" with a variety of materials on a nonporous scale. Great flexibility is afforded by this material's processing technique because of the variety of backbone structures that can be produced and the ability to incorporate a large variety of additional constituents.[7,8] This can be accomplished by modifying or adding functional groups to the sol gel precursor, or by chemical vapor infiltration (CVI) after the solvent has been extracted from the pores. CVI is chemically similar to chemical vapor deposition, CVD, but occurs inside a porous material. Using these techniques, it is possible to use substantial amounts of materials to coat the backbone with several times its volume. Thus, this approach to building mesoporous materials offers a flexible and cost effective route to a variety of materials tailored at the nanoscale for hydrogen storage as well as other applications.

We have been investigating the preparation and properties of ultra-low density nanomaterials based on aerogel technology since 1980. We also developed a technique to substitute nonflammable carbon dioxide for alcohol in the gel and perform the supercritical drying at lower temperatures (31.1°C and 73.0 bars).[9] A wide variety of aerogel compositions have been prepared including metal oxides (SiO_2, TiO_2, Fe_3O_4, Al_2O_3, MgO, Cr_2O_3, Zr_2O_3), mixed oxides, and other compounds.[10] Many of these have had additional coatings or deposits using pre- and post-supercritical drying treatments.[11,12] A wide variety of elements and compounds have been deposited using sol-gel chemistry, solvent additions and Chemical Vapor Infiltration. The most widely investigated combination is silica aerogel coated with carbon using CVI with acetylene. **Figure 1** illustrates a pure silica aerogel and a carbon doped silica aerogel. As a measure of the effectiveness of this process we have achieved from 1% to 400% loading of carbon into the silica (four times more carbon mass than silica).

Figure 1. Photographs showing un-doped (left) and carbon-doped (right) ultra-low density SiO_2 network material.

Mesoporous Oxides for Hydrogen Storage

One of the key advantages of using ultralow density ceramic materials arises because of the size of the pores and the composition and functionality of the oxide backbone materials. Aerogels can be readily modified by changing the synthesis parameters. One modification approach is to vary the mixtures of precursors during preparation (the sol-gel stage). For instance, one can dope $Si(OAlk)_4$ (**Aldrich Prod. Nos.** 679321, 679259, 679240, T5702, 333859) or $Ti(OAlk)_4$ (**Aldrich Prod. Nos.** 252670, 244112, 462551, 244759, 333484, 377996, 463582, 253081) with transition metal salts or boron compounds. During hydrolysis, transition metals can be incorporated into the oxide network. If functionalized dopants are employed, such as *A*-CH_2-$Si(OAlk)_3$ (**Aldrich Prod. Nos.** 679267, 679356, 679291, 679275) or $(A\text{-}CH_2)_2Si(OAlk)_2$ (**Aldrich Prod. Nos.** 371890, 435171, 539260, 446173), one can introduce additional chemisorption centers in the oxide network materials by coordinating *A* to transition metals (added after the network structure is formed). Additionally, the network material properties can be tuned by varying the compositions of the coatings, which would lead to applications far beyond hydrogen storage.

Once the mesoporous oxide networks are prepared, several approaches can be used to modify them. An example of the modification strategy, used to prepare *X*-SiO_2 porous networks, is depicted in **Figure 2,** where *X* may be a high-capacity hydride compound, intercalated within the array of SiO_2 nanoparticles of the aerogel, and filling a significant fraction of the pore space.

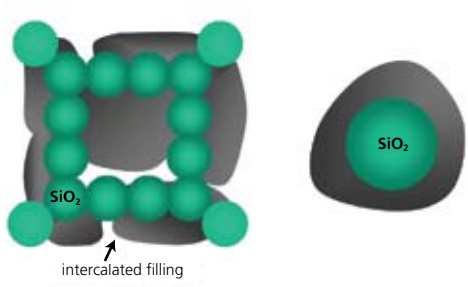

Figure 2. Schematic illustration of a strategy of modified active oxide networks. The right illustration represents individual hydride-X coated oxide nanostructure, forming an X-SiO_2.

A schematic illustration (in two-dimensional projection plane) of the ultralow-density oxide network material is given in **Figure 3a.** It consists of a network of silica nanoparticles, approximately 3 nm in diameter, with a system of nanopores far smaller than the wavelength of visible light, typically 10 nm. **Figure 3b** is a transmission electron microscopy (TEM) image of a synthesized sample, illustrating that the highly porous medium consists of a network of randomly positioned silica nanoparticles. The specific surface area of the un-coated silica network is typically 1000 m^2/g as measured by BET, and the bulk density is about 0.08 g/cm^3.

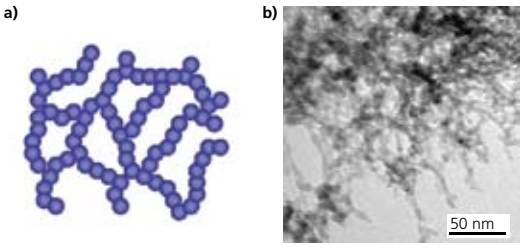

Figure 3. (a) Schematic illustration of a material consisting of a network of silica nanoparticles (b) TEM image of an ultralow-density silica oxide network sample.

We investigated the baseline properties of SiO_2 ceramic nanoparticle networks for hydrogen storage to better understand and evaluate the effects of further modification of the materials. We found the SiO_2 nanoparticle networks have favorable hydrogen storage properties through physisorption due to their very large surface area. Nevertheless, the storage capacity of the network does not yet meet the US DOE's gravimetric and volumetric targets. The adsorbed capacity of an ultralow density silica network at liquid nitrogen temperature is shown in **Figure 4**. Measurements were conducted using a volumetric hydrogen storage testing system (PCTPro, Hy-Energy; see reference 13 for details). It can be seen that the hydrogen adsorption capacity increases monotonically to 40 bar and continues to rise with pressure.

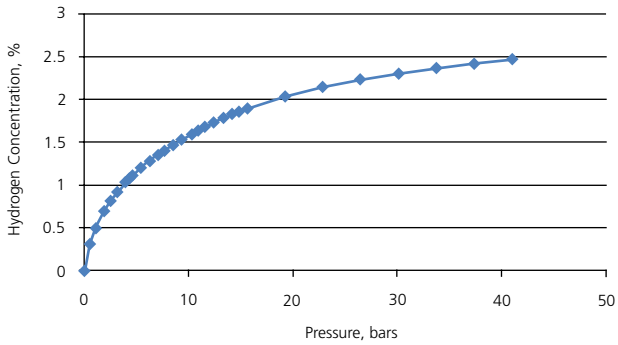

Figure 4. Hydrogen storage capacity of ultralow density silicon network vs. pressure in bars.

To increase the density of stored hydrogen we introduce chemisorption into this system, while maintaining the benefit of the high-surface area for additional storage through functionalized physisorption. At the same time, the high-surface area nanoparticle network should provide the additional benefit of markedly improved chemisorption kinetics by increasing reaction surface area as well, as reducing diffusion distance (of hydrogen as well as constituent reactants).

As a proof of concept experiment, we fabricated a composite material using MgNi (<5 wt.%) implemented in an ultralow-density SiO_2 aerogel nanoparticle network. Using magnesium, a structure was formed with 7.6 wt.% hydride, MgH_2 (**Aldrich Prod. No. 683043**), but is generally hindered by poor kinetics caused by limited diffusion of hydrogen through the hydride. Ni is an effective catalyst for hydrogen dissociation and when combined with Mg may form the intermetallic compound Mg_2Ni which also forms a hydrogen-rich complex hydride Mg_2NiH_4.

The composite network was prepared by a two-step process, starting with the pH-dependent hydrolysis and condensation of an alkoxysilane in alcohol, followed by CO_2 substitution and supercritical drying. Under a high vacuum environment, the resulting SiO_2 nanoparticle network was subjected to vapor infiltration of Mg and Ni through the use of a physical or a chemical vapor deposition process (we used a pulsed laser to vaporize a solid state MgNi alloy target). Preliminary measurements indicate chemisorption of hydrogen in the modified silica network, in addition to physisorption due to the very large surface area offered by the oxide network.

A technological advantage presented by the modified active oxide networks is their scalability. We have demonstrated large scale manufacturing feasibility of nanostructured oxide networks based on supercritical drying/sol-gel process and chemical vapor infiltration/deposition for incorporating desired compound through the mesopores of the oxide network. These ultralow density materials can be fabricated with varying density, structure and shape. Monolithic squares up to 20 inches on a side have been synthesized at Berkeley; they would be suitable for on-board transportation applications. With this scale-up manufacturing possibility, ultralow density active ceramic networks represent a clear alternative to existing porous media for solid-state hydrogen storage.

Summary

The above proof-of-concept experiments and analyses demonstrate the potential of the ultralow-density modified active oxide networks. While the hydrogen storage capacity of the mesoporous ceramic networks are not yet sufficient, it is our goal to modify them in order to achieve desired hydrogen storage capacity and kinetics. The optimized performance of the new materials can be realized by process modifications that include tuning the structure and specific surface area of the active oxide networks and implementing different combinations of catalytic and chemisorbing phases.

References:

(1) Satyapal, S.; Petrovic, J.; Read, C.; Thomas, G.; Ordaz, G. *Catalysis Today* **2007**, *120*, 246.
(2) Schlapbach, L.; Zuttel, A. *Nature* **2001**, *414*, 353.
(3) Bogdanovic, B.; Sandrock, G. **2002** *MRS Bulletin, September* 712.
(4) Rosi, N.L.; Eckert, J.; Eddaoudi, M.; Vodak, D.T.; Kim, J.; O'Keeffe, M.; Yaghi, O.M. *Science* **2003** *300*, 1127.
(5) Rowsell, J.L.C.; Yaghi, O.M. *Angew. Chem. Int. Ed.* **2005**, *44,* 4670.
(6) Kistler, S.S. *Nature*, **1931** *227*, 741.
(7) Mao, S. S.; Carrington, K. R.; Chen, X.; Hunt, A.; Gross, K., Hydrogen storage in ultra-low density silica aerogel, private communication.
(8) Ayers, M.R.; Song, X.Y.; Hunt, A.J. *J. Mat. Sci.* **1996** *31*, 6251.
(9) Tewari, P.H.; Hunt, A.J.; Lofftus, K.D. *Mat. Lett.* **1985** *3*, 363.
(10) Hunt, A. *Encyclopedia Britannica Science Year Book*, **1996** 146.
(11) Hunt, A.J.; Ayers, M.R.; Cao, W. *J. Non-Cryst. Solids* **1995** *185,* 227.
(12) Balema, V. P. *Material Matters* **2006** *1,* 3.
(13) Gross, K. *Material Matters* **2006**, *2*, 2, 26.

Chloro- and Alkoxysilanes

For a complete list of sol-gel precursors, please visit ***sigma-aldrich.com/solgel***

Name	Structure	Purity	Physical Form	Cat. No.
Pentyltrichlorosilane	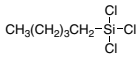	≥98% deposition grade	liquid	679194-50G
Methyltrichlorosilane		≥98%, GC ≥99.99% (as metals) deposition grade	liquid	679208-50G
Ethyltrichlorosilane		≥98%, GC ≥99.99% (as metals) deposition grade	liquid	679216-50G
Butyltrichlorosilane	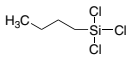	≥98% deposition grade	liquid	679224-50G
Trimethoxymethylsilane		≥98% deposition grade	liquid	679232-50G
Tetrapropyl orthosilicate	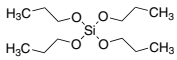	≥98% deposition grade	liquid	679240-50G
Tetramethyl orthosilicate	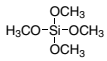	≥99.9% trace metals basis ≥98% deposition grade	liquid	679259-50G
Allyltrimethoxysilane	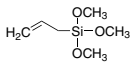	≥98% deposition grade	liquid	679267-50G
Triethoxyvinylsilane	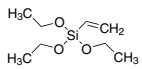	≥98% deposition grade	liquid	679275-50G
Triethoxyphenylsilane	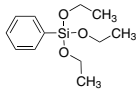	≥98% deposition grade	liquid	679291-50G
Triethoxy(octyl)silane	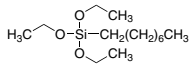	99.99% trace metals basis 98% deposition grade	liquid	679305-50G
Trimethoxyphenylsilane	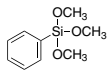	≥98% deposition grade	liquid	679313-50G
n-Propyltriethoxysilane	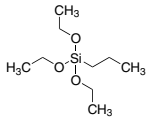	≥98% deposition grade	liquid	679321-50G
[3-(Diethylamino)propyl]trimethoxysilane	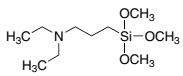	≥98% deposition grade	liquid	679356-50G
Isobutyl(trimethoxy)silane	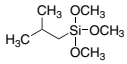	≥98% deposition grade	solution	679364-50G

Metal Alkoxides

For a complete list of sol-gel precursors, please visit ***sigma-aldrich.com/solgel***

Name	Structure	Purity/Concentration	Physical Form	Cat. No.
Magnesium acetate	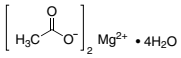	99.999% trace metals basis	solid	229768-10G 229768-100G
Magnesium acetylacetonate	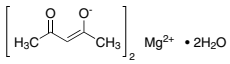	98%	solid	129577-25G
Magnesium methoxide	$Mg(OCH_3)_2$	6-10 wt. % in methanol	-	335657-500ML 335657-2L
Magnesium ethoxide	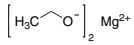	98%	granular	291846-100G 291846-500G
Aluminum acetylacetonate	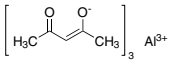	99.999%	solid	674753-5G 674753-25G
Aluminum phenoxide	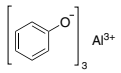	99.9% trace metals basis	solid	495131-5G 495131-25G
Aluminum-tri-*sec*-butoxide	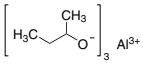	97%	liquid	201073-5G 201073-100G 201073-500G
Titanium(IV) isopropoxide	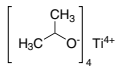	97%	liquid	205273-5ML 205273-100ML 205273-500ML 205273-2L
Aluminum acetylacetonate	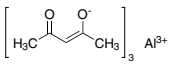	99%	solid	208248-5G 208248-100G 208248-500G
Aluminum isopropoxide	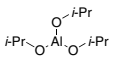	≥99.99% trace metals basis	solid	229407-10G 229407-50G 229407-250G
Aluminum isopropoxide	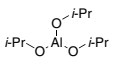	≥98%	solid	220418-100G 220418-1KG
Aluminum *tert*-butoxide	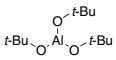	-	powder	235849-10G 235849-50G
Aluminum ethoxide	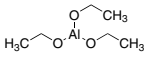	97%	solid	235857-5G 235857-25G 235857-100G
Aluminum acetate, basic	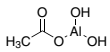	-	powder	294853-250G 294853-1KG
Diethylaluminum ethoxide		97%	liquid	256749-100G
Aluminum tributoxide	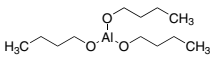	95%	solid	403350-5G 403350-25G
Aluminum-tri-*sec*-butoxide	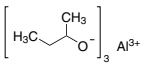	99.99% trace metals basis	liquid	511609-5G
Aluminum tri-*sec*-butoxide	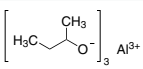	1.0 M in methylene chloride	solution	558907-500ML
Titanium(IV) methoxide	$Ti(OCH_3)_4$	≥99.99% trace metals basis	solid	463582-25G
Titanium(IV) methoxide	$Ti(OCH_3)_4$	95%	solid	404950-10G 404950-50G
Titanium(IV) ethoxide	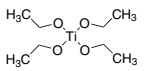	-	liquid	244759-50G 244759-250G
Titanium(IV) butoxide	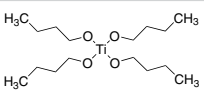	97%	liquid	244112-5G 244112-100G 244112-500G 244112-2KG

Name	Structure	Purity/Concentration	Physical Form	Cat. No.
Titanium(IV) *tert*-butoxide	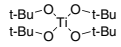	-	liquid	462551-25ML 462551-50ML
Titanium(IV) propoxide	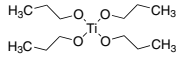	98%	liquid	253081-100G 253081-500G
Titanium(IV) isopropoxide	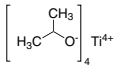	99.999% trace metals basis	liquid	377996-5ML 377996-25ML 377996-100ML
Titanium diisopropoxide bis(acetylacetonate)	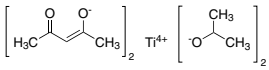	75 wt. % in isopropanol	solution	325252-100ML 325252-500ML
Titanium(IV) oxide acetylacetonate	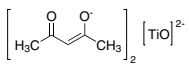	95%	powder	330833-10G 330833-50G
Titanium(IV) 2-ethylhexyloxide	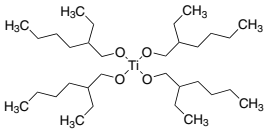	95%	liquid	333484-250ML
Chlorotriisopropoxytitanium(IV)	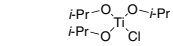	95%	liquid	250627-100G 250627-800G
Chlorotriisopropoxytitanium(IV)	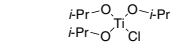	1.0 M in hexanes	solution	252670-100ML 252670-800ML
Zirconium(IV) ethoxide	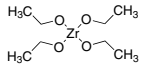	97%	solid	339121-5G 339121-25G
Zirconium(IV) butoxide	$Zr(OCH_2CH_2CH_2CH_3)_4$	80 wt. % in 1-butanol	solution	333948-100ML 333948-500ML 333948-2L
Zirconium(IV) *tert*-butoxide	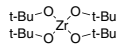	99.999% trace metals basis	liquid	560030-5G 560030-25G
Zirconium(IV) propoxide	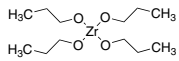	70 wt. % in 1-propanol	solution	333972-100ML 333972-500ML
Zirconium(IV) isopropoxide isopropanol complex	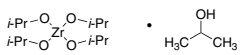	99.9% trace metals basis	powder	339237-10G 339237-50G
Zirconium acetate	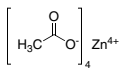	in dilute acetic acid	liquid	413801-500ML 413801-2L
Zirconium(IV) acetate hydroxide	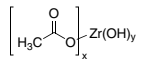	-	powder	464600-100G 464600-500G
Zirconium(IV) acetylacetonate	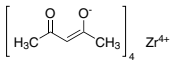	98%	powder	338001-25G 338001-100G
Zirconium(IV) trifluoroacetylacetonate	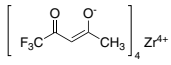	97%	solid	383325-1G
Zirconium(IV) bis(diethyl citrato) dipropoxide	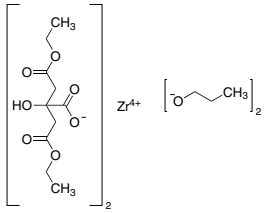	-	liquid	515817-1L

Titanates

Name	Formula	Purity	Dimensions	Physical Form	Cat. No.
Lithium titanate	Li_2TiO_3	-	–325 mesh	powder	400939-100G 400939-500G
Lithium titanate, spinel	$Li_4Ti_5O_{12}$	>99%	particle size <100 nm TEM) particle size <100 nm BET)	nanopowder	702277-25G
Aluminum titanate	$Al_2O_3{\cdot}TiO_2$	98.5% trace metals basis	particle size <25 nm BET)	nanopowder	634131-20G 634131-100G
Aluminum titanate	$Al_2O_3{\cdot}TiO_2$	-	-	powder	520209-250G
Titanium silicon oxide	$(SiO_2)(TiO_2)$	99.8% trace metals basis	particle size <50 nm BET)	nanopowder	641731-10G 641731-50G
Calcium titanate	$CaTiO_3$	99.9% trace metals basis	particle size <100 nm BET) particle size <50 nm XRD)	nanopowder	633801-25G 633801-100G
Calcium titanate	$CaTiO_3$	99%	–325 mesh	powder	372609-2KG
Iron(II) titanate	$FeTiO_3$	99.9%	–100 mesh	powder	400874-25G 400874-100G
Zinc titanate	$ZnTiO_4 \cdot ZnTiO_2$	99.5% trace metals basis	particle size <100 nm BET) particle size <50 nm XRD)	nanopowder	634409-25G 634409-100G
Strontium titanate	$SrTiO_3$	≥99.5% trace metals basis	particle size <100 nm	nanopowder	517011-50G
Strontium titanate	$SrTiO_3$	99%	5 µm	powder	396141-100G 396141-500G
Strontium titanate	$SrTiO_3$	≥99.99% trace metals basis	10 × 10 × 0.5 mm	<110> single crystal substrate single side polished crystalline (cubic (a = 3.905 Å))	634670-1EA
Strontium titanate	$SrTiO_3$	99.99% trace metals basis	10 × 10 × 0.5 mm	<111> single crystal substrate single side polished	638161-1EA
Strontium titanate	$SrTiO_3$	-	10 × 10 × 0.5 mm	<100> single crystal substrate crystalline (cubic (a=3.905 Å))	634689-1EA
Barium titanate(IV)	$BaTiO_3$	99.995% trace metals basis	-	powder	256552-10G 256552-50G
Barium titanate(IV)	$BaTiO_3$	≥99% trace metals basis	particle size <100 nm BET)	nanopowder (cubic crystalline phase)	467634-25G 467634-100G
Barium titanate(IV)	$BaTiO_3$	99.9% trace metals basis	3 - 12 mm	pieces sintered	342939-50G
Barium titanate(IV)	$BaTiO_3$	99.9% trace metals basis	<2 µm	powder	338842-100G 338842-500G
Barium titanate(IV)	$BaTiO_3$	99%	<3 µm	powder	208108-500G 208108-2KG
Barium titanate(IV)	$BaTiO_3$	≥98.0%	particle size <3 µm	powder	11848-1KG
Neodymium(III) titanate	$2Nd_2O_3 \cdot 5TiO_2$	-	–325 mesh	powder	403695-500G
Lead(II) titanate	$PbTiO_3$	≥99%	<5 µm	powder	215805-250G
Bismuth(III) titanate	$Bi_2O_3{\cdot}2TiO_2$	-	–325 mesh	powder	403687-100G

Tungstates

Name	Formula	Purity	Dimensions	Physical Form	Cat. No.
Lithium tungstate	Li_2WO_4	98%	-	powder	400912-25G 400912-100G
Ammonium tungstate	$(NH_4)_{10}H_2(W_2O_7)_6$	99.99% trace metals basis	-	powder	322385-10G 322385-50G
Sodium tungstate	$Na_2WO_4 \cdot 2H_2O$	99.995% trace metals basis	-	chunks	379751-5G 379751-25G
Sodium phosphotungstate	$Na_3PO_4{\cdot}12WO_3{\cdot}xH_2O$	≥99.9% trace metals basis	-	powder	496626-25G 496626-100G
Sodium phosphotungstate	$\sim 2Na_2O{\cdot}P_2O_5{\cdot}12WO_3{\cdot}18H_2O$	-	-	powder	P6395-25G P6395-100G P6395-500G
Magnesium tungstate	$MgWO_4$	99.9% trace metals basis	–325 mesh	powder	415073-10G 415073-50G
Potassium tungstate	K_2WO_4	≥99.99% trace metals basis	-	powder	483079-5G 483079-25G
Potassium tungstate	K_2WO_4	94%	–100 mesh	powder	372617-100G
Calcium tungstate	$CaWO_4$	-	-	powder	248665-100G 248665-500G
Strontium tungsten oxide	$SrWO_4$	99.9% trace metals basis	–200 mesh	powder	709220-10G
Silver tungstate	Ag_2WO_4	99.99% trace metals basis	-	powder	587362-10G
Cadmium tungstate	$CdWO_4$	-	–325 mesh	powder	401129-5G 401129-25G
Barium tungstate	$BaWO_4$	99.9% trace metals basis	–100 mesh	powder	343137-50G
Barium yttrium tungsten oxide	$Ba_3Y_2WO_9$	99.9%	<5 µm	powder	415170-25G
Bismuth tungsten oxide	$Bi_2(WO_4)_3$	-	–200 mesh	powder	709239-10G

Zirconates

Name	Formula	Purity	Dimensions	Physical Form	Cat. No.
Lithium zirconate	Li_2ZrO_3	-	–80 mesh	powder	400920-25G 400920-100G
Sodium zirconate	Na_2ZrO_3	-	–200 mesh	powder	400661-5G 400661-25G
Calcium zirconate	$CaZrO_3$	99.7% trace metals basis	particle size <25 nm XRD) particle size <50 nm BET)	nanopowder	631965-25G 631965-100G
Strontium zirconate	$SrZrO_3$	-	10 µm	powder	396168-250G
Barium zirconate	$BaZrO_3$	98.5% trace metals basis	particle size <50 nm	nanopowder	631884-25G 631884-100G
Barium zirconate	$BaZrO_3$	-	<10 µm	powder	383309-250G
Lead(II) zirconate	$PbZrO_3$	99% trace metals basis	–325 mesh	powder	398888-50G 398888-250G

Niobates

Name	Formula	Purity	Dimensions	Physical Form	Cat. No.
Lithium niobate	$LiNbO_3$	99.9% trace metals basis	200 mesh	powder	254290-10G 254290-100G
Ammonium fluoroniobate	$^5[NH_4^+]\ [Nb(O)F_4^-2NbF_7^{2-}]$	99.99%	-	powder	525707-10G
Sodium niobate	$NaNbO_3$	99.9%	–100 mesh	powder	400653-5G 400653-25G
Potassium niobate	$KNbO_3$	-	-	powder	541206-25G
Potassium heptafluoroniobate(V)	K_2NbF_7	98%	-	powder	336645-25G
Zinc niobate	$Zn(NbO_3)_2$	97%	-	powder	548588-50G
Lead magnesium niobate	$(PbO)_3(MgO)(Nb_2O_5)$	≥99%	-	powder	672874-25G

Aldrich Materials for Solid Oxide Fuel Cell Applications

A fuel cell is a battery-like system that uses hydrogen and oxygen to generate electricity by an electrochemical reaction. Similar to other batteries, the fuel cell consists of two electrodes (porous anode and cathode) and an electrolyte (**Figure 1**).

In Solid Oxide Fuel Cells (SOFCs), the cathode and the anode are made from porous ceramic materials and the electrolyte consists of a dense oxygen ion conducting ceramic. This allows SOFCs to operate at high temperatures around 1,000°C (1,830°F) and to reform hydrocarbons internally, thus enabling the use of natural gas or reformed diesel as fuel.[1]

The high-temperature operation places rigorous durability requirements on cell components. Therefore development of low-cost materials with high durability at high temperatures is the key technical challenge for SOFC technology.[2]

Aldrich Materials Science offers a variety of materials that can be used for the preparation of cathodes, anodes and electrolytes for SOFC applications. Our product portfolio includes a variety of Yttria Stabilized Zirconia (YSZ), Lanthanum Strontium Manganite (LSM), Gadolinium doped Ceria (GDC) and other ceramic materials specifically designed for SOFC applications.

For complete list of our fuel cell materials and related products, please visit *sigma-aldrich.com/energy*

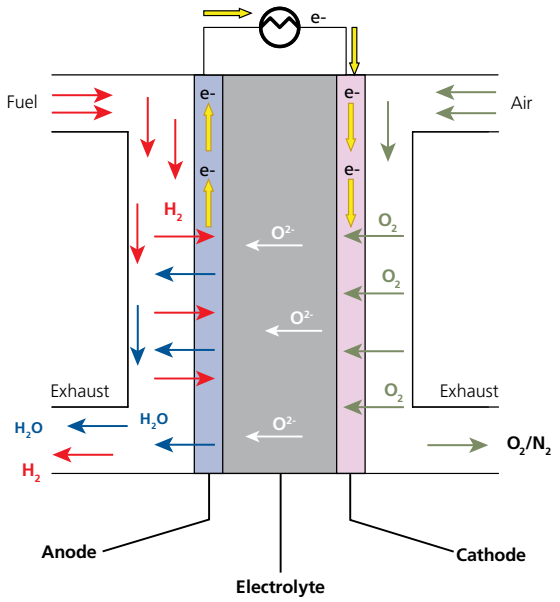

References:

1 *High Temperature and Solid Oxide Fuel Cells. Fundamentals, Design and Applications;* Singhal, S.C., Kendal, K. Eds.; Elsevier: Amsterdam, The Netherlands, 2003.

2. *U.S. Department of Energy. Energy Efficiency and Renewable Energy. The Hydrogen, Fuel Cells & Infrastructure Technologies Program.* www1.eere.energy.gov/ hydrogenandfuelcells/ fuelcells/ (last accessed May 5, 2009)

Cathode Materials

Material Name	Composition	Cat. No.
Lanthanum strontium manganite	$(La_{0.80}Sr_{0.20})_{0.95}MnO_3$, 50% $Ce_{0.9}Gd_{0.1}O_{1.95}$, 50%	704237-10G
Lanthanum strontium manganite, ≥99%	$(La_{0.80}Sr_{0.2})MnO_3$, 50% $(Y_2O_3)_{0.08}(ZrO_2)_{0.92}$, 50%	704245-10G
Lanthanum strontium cobalt ferrite	$(Ce_{0.9}Gd_{0.1})O_{1.95}$, 50% $(La_{0.60}Sr_{0.40})(Co_{0.20}Fe_{0.80})O_3$, 50%	704253-10G
Lanthanum strontium manganite, ≥99%	$(Ce_{0.9}Gd_{0.1})O_{1.95}$, 50% $(La_{0.80}Sr_{0.20})MnO_3$, 50%	704296-10G

Anode Materials

Material Name	Composition	Cat. No.
Nickel oxide - Yttria-stabilized zirconia	Nickel oxide, 66 wt. % Yttria-stabilized zirconia, 34 wt. %	704202-10G
Nickel oxide - Cerium samarium oxide, ≥99% trace metals basis	Cerium Samarium Oxide, 40 wt. % Nickel Oxide, 60 wt. %	704210-10G

Electrolytes

Material Name	Composition	Cat. No.
Zirconium(IV) oxide-yttria stabilized	O_2Zr/yttria 3% as stabilizer	572322-25G
Zirconium(IV) oxide-yttria stabilized	O_2Zr/yttria ~8% as stabilizer	464228-100G 464228-500G
Zirconium(IV) oxide-yttria stabilized	O_2Zr/yttria ~5.3% as stabilizer	464201-100G 464201-500G
Cerium(IV) oxide-gadolinium doped	CeO_2/gadolinium 10 mol % as dopant	572330-25G
Zirconium(IV) oxide-yttria stabilized	O_2Zr/yttria 8% as stabilizer	572349-25G
Cerium(IV) oxide-gadolinium doped	CeO_2/gadolinium 20 mol % as dopant	572357-25G
Cerium(IV) oxide-samaria doped	CeO_2/samaria 15 mol % as dopant	572365-25G
Cerium(IV) oxide-yttria doped	CeO_2/yttria 15 mol % as dopant	572381-25G

Sigma-Aldrich
3050 Spruce Street
St. Louis, MO 63103 USA
sigma-aldrich.com

Argentina
SIGMA-ALDRICH DE ARGENTINA S.A.
Free Tel: 0810 888 7446
Tel: (+54) 11 4556 1472
Fax: (+54) 11 4552 1698

Australia
SIGMA-ALDRICH PTY LTD.
Free Tel: 1800 800 097
Free Fax: 1800 800 096
Tel: (+61) 2 9841 0555
Fax: (+61) 2 9841 0500

Austria
SIGMA-ALDRICH HANDELS GmbH
Tel: (+43) 1 605 81 10
Fax: (+43) 1 605 81 20

Belgium
SIGMA-ALDRICH NV/S.A.
Free Tel: 0800 14747
Free Fax: 0800 14745
Tel: (+32) 3 899 13 01
Fax: (+32) 3 899 13 11

Brazil
SIGMA-ALDRICH BRASIL LTDA.
Free Tel: 0800 701 7425
Tel: (+55) 11 3732 3100
Fax: (+55) 11 5522 9895

Canada
SIGMA-ALDRICH CANADA LTD.
Free Tel: 1800 565 1400
Free Fax: 1800 265 3858
Tel: (+1) 905 829 9500
Fax: (+1) 905 829 9292

Chile
SIGMA-ALDRICH
QUIMICA LIMITADA
Tel: (+56) 2 495 7395
Fax: (+56) 2 495 7396

China
SIGMA-ALDRICH (SHANGHAI)
TRADING CO. LTD.
Free Tel: 800 819 3336
Tel: (+86) 21 6141 5566
Fax: (+86) 21 6141 5567

Czech Republic
SIGMA-ALDRICH spol. s r. o.
Tel: (+420) 246 003 200
Fax: (+420) 246 003 291

Denmark
SIGMA-ALDRICH DENMARK A/S
Tel: (+45) 43 56 59 00
Fax: (+45) 43 56 59 05

Finland
SIGMA-ALDRICH FINLAND OY
Tel: (+358) 9 350 9250
Fax: (+358) 9 350 92555

France
SIGMA-ALDRICH CHIMIE S.à.r.l.
Free Tel: 0800 211 408
Free Fax: 0800 031 052
Tel: (+33) 474 82 28 00
Fax: (+33) 474 95 68 08

Germany
SIGMA-ALDRICH CHEMIE GmbH
Free Tel: 0800 51 55 000
Free Fax: 0800 64 90 000
Tel: (+49) 89 6513 0
Fax: (+49) 89 6513 1160

Greece
SIGMA-ALDRICH (O.M.) LTD.
Tel: (+30) 210 994 8010
Fax: (+30) 210 994 3831

Hungary
SIGMA-ALDRICH Kft
Ingyenes telefonszám: 06 80 355 355
Ingyenes fax szám: 06 80 344 344
Tel: (+36) 1 235 9055
Fax: (+36) 1 235 9050

India
SIGMA-ALDRICH CHEMICALS
PRIVATE LIMITED
Telephone
Bangalore: (+91) 80 6621 9400
New Delhi: (+91) 11 4358 8000
Mumbai: (+91) 22 2570 2364
Hyderabad: (+91) 40 4015 5488
Kolkata: (+91) 33 4013 8003
Fax
Bangalore: (+91) 80 6621 9650
New Delhi: (+91) 11 4358 8001
Mumbai: (+91) 22 2579 7589
Hyderabad: (+91) 40 4015 5466
Kolkata: (+91) 33 4013 8016

Ireland
SIGMA-ALDRICH IRELAND LTD.
Free Tel: 1800 200 888
Free Fax: 1800 600 222
Tel: (+353) 402 20370
Fax: (+ 353) 402 20375

Israel
SIGMA-ALDRICH ISRAEL LTD.
Free Tel: 1 800 70 2222
Tel: (+972) 8 948 4100
Fax: (+972) 8 948 4200

Italy
SIGMA-ALDRICH S.r.l.
Numero Verde: 800 827018
Tel: (+39) 02 3341 7310
Fax: (+39) 02 3801 0737

Japan
SIGMA-ALDRICH JAPAN K.K.
Tel: (+81) 3 5796 7300
Fax: (+81) 3 5796 7315

Korea
SIGMA-ALDRICH KOREA
Free Tel: (+82) 80 023 7111
Free Fax: (+82) 80 023 8111
Tel: (+82) 31 329 9000
Fax: (+82) 31 329 9090

Malaysia
SIGMA-ALDRICH (M) SDN. BHD
Tel: (+60) 3 5635 3321
Fax: (+60) 3 5635 4116

Mexico
SIGMA-ALDRICH QUÍMICA, S.A. de C.V.
Free Tel: 01 800 007 5300
Free Fax: 01 800 712 9920
Tel: (+52) 722 276 1600
Fax: (+52) 722 276 1601

The Netherlands
SIGMA-ALDRICH CHEMIE BV
Free Tel: 0800 022 9088
Free Fax: 0800 022 9089
Tel: (+31) 78 620 5411
Fax: (+31) 78 620 5421

New Zealand
SIGMA-ALDRICH NEW ZEALAND LTD.
Free Tel: 0800 936 666
Free Fax: 0800 937 777
Tel: (+61) 2 9841 0555
Fax: (+61) 2 9841 0500

Norway
SIGMA-ALDRICH NORWAY AS
Tel: (+47) 23 17 60 00
Fax: (+47) 23 17 60 10

Poland
SIGMA-ALDRICH Sp. z o.o.
Tel: (+48) 61 829 01 00
Fax: (+48) 61 829 01 20

Portugal
SIGMA-ALDRICH QUÍMICA, S.A.
Free Tel: 800 202 180
Free Fax: 800 202 178
Tel: (+351) 21 924 2555
Fax: (+351) 21 924 2610

Russia
SIGMA-ALDRICH RUS, LLC
Tel: (+7) 495 621 5579
Fax: (+7) 495 621 5923

Singapore
SIGMA-ALDRICH PTE. LTD.
Tel: (+65) 6779 1200
Fax: (+65) 6779 1822

Slovakia
SIGMA-ALDRICH spol. s r. o.
Tel: (+421) 255 571 562
Fax: (+421) 255 571 564

South Africa
SIGMA-ALDRICH (PTY) LTD.
Free Tel: 0800 1100 75
Free Fax: 0800 1100 79
Tel: (+27) 11 979 1188
Fax: (+27) 11 979 1119

Spain
SIGMA-ALDRICH QUÍMICA, S.A.
Free Tel: 900 101 376
Free Fax: 900 102 028
Tel: (+34) 91 661 99 77
Fax: (+34) 91 661 96 42

Sweden
SIGMA-ALDRICH SWEDEN AB
Tel: (+46) 8 742 4200
Fax: (+46) 8 742 4243

Switzerland
SIGMA-ALDRICH CHEMIE GmbH
Free Tel: 0800 80 00 80
Free Fax: 0800 80 00 81
Tel: (+41) 81 755 2828
Fax: (+41) 81 755 2815

United Kingdom
SIGMA-ALDRICH COMPANY LTD.
Free Tel: 0800 717 181
Free Fax: 0800 378 785
Tel: (+44) 1747 833 000
Fax: (+44) 1747 833 313

United States
SIGMA-ALDRICH
Toll-Free: 800 325 3010
Toll-Free Fax: 800 325 5052
Tel: (+1) 314 771 5765
Fax: (+1) 314 771 5757

Vietnam
SIGMA-ALDRICH PTE LTD. VN R.O.
Tel: (+84) 3516 2810
Fax: (+84) 6258 4238

Internet
sigma-aldrich.com

Green U Power

FSC Mixed Sources
Product group from well-managed forests, controlled sources and recycled wood or fiber
www.fsc.org Cert no. SGS-COC-003338
© 1996 Forest Stewardship Council
10%

World Headquarters
3050 Spruce St., St. Louis, MO 63103
(314) 771-5765
sigma-aldrich.com

Order/Customer Service (800) 325-3010 • Fax (800) 325-5052
Technical Service (800) 325-5832 • *sigma-aldrich.com/techservice*
Development/Custom Manufacturing Inquiries SAFC® (800) 244-1173

*Accelerating Customers' Success through Innovation and Leadership in **Life Science**, **High Technology** and **Service***

LJI
71457-508473
0059

SIGMA-ALDRICH®